2012

Integration of a high sensitivity MEMS directional sound sensor with readout electronics

Roth, John D.

Monterey, California. Naval Postgraduate School

NAVAL POSTGRADUATE SCHOOL

MONTEREY, CALIFORNIA

THESIS

INTEGRATION OF A HIGH SENSITIVITY MEMS DIRECTIONAL SOUND SENSOR WITH READOUT ELECTRONICS

by

John D. Roth

December 2012

Thesis Advisor:	Gamani Karunasiri
Co-Advisor:	Douglas J. Fouts

THIS PAGE INTENTIONALLY LEFT BLANK

REPORT DOCUMENTATION PAGE			Form Approved OMB No. 0704–0188

1. AGENCY USE ONLY *(Leave blank)*	2. REPORT DATE December 2012	3. REPORT TYPE AND DATES COVERED Master's Thesis

4. TITLE AND SUBTITLE Integration of a High Sensitivity MEMS Directional Sound Sensor with Readout Electronics	5. FUNDING NUMBERS
6. AUTHOR(S) John D. Roth	
7. PERFORMING ORGANIZATION NAME(S) AND ADDRESS(ES) Naval Postgraduate School Monterey, CA 93943–5000	8. PERFORMING ORGANIZATION REPORT NUMBER
9. SPONSORING /MONITORING AGENCY NAME(S) AND ADDRESS(ES) Space and Naval Warfare Systems Command	10. SPONSORING/MONITORING AGENCY REPORT NUMBER

11. SUPPLEMENTARY NOTES The views expressed in this thesis are those of the author and do not reflect the official policy or position of the Department of Defense or the U.S. Government. IRB Protocol number _____N/A_____.

12a. DISTRIBUTION / AVAILABILITY STATEMENT Approved for public release; distribution is unlimited	12b. DISTRIBUTION CODE

13. ABSTRACT (maximum 200 words)

The miniaturization of a sound detection system is of great interest to applications such as sniper location. Current systems in use are larger and do not provide for the unencumbered movement of the warfighter. Inspiration for a smaller MEMS based sensor is therefore taken from the aural system of the fly Ormia ochracea. The focus of this thesis is the design of an integrated and miniaturized device utilizing commercial-off-the-shelf readout electronics with the biologically inspired sensor. An analysis of previously used techniques is presented along with a novel fully-integrated miniaturized design. Specific investigations include integration with external readout electronics, a hybrid discrete component design, and the fully-integrated single package design. Results include successful operation at all levels of integration and a more thorough analysis of the performance of the fully-integrated design.

14. SUBJECT TERMS MEMS, Directional Microphones, Sniper Detection, Capacitive Readout, Switched Capacitor	15. NUMBER OF PAGES 78
	16. PRICE CODE

17. SECURITY CLASSIFICATION OF REPORT	18. SECURITY CLASSIFICATION OF THIS PAGE	19. SECURITY CLASSIFICATION OF ABSTRACT	20. LIMITATION OF ABSTRACT
Unclassified	Unclassified	Unclassified	UU

NSN 7540–01–280–5500

Standard Form 298 (Rev. 2–89)
Prescribed by ANSI Std. 239–18

THIS PAGE INTENTIONALLY LEFT BLANK

Approved for public release; distribution is unlimited

INTEGRATION OF A HIGH SENSITIVITY MEMS DIRECTIONAL SOUND SENSOR WITH READOUT ELECTRONICS

John D. Roth
Captain, United States Marine Corps
B.S., United States Naval Academy, 2004

Submitted in partial fulfillment of the
requirements for the degree of

MASTER OF SCIENCE IN ELECTRICAL ENGINEERING

from the

NAVAL POSTGRADUATE SCHOOL
December 2012

Author: John D. Roth

Approved by: Gamani Karunasiri
Thesis Advisor

Douglas J. Fouts
Co-Advisor

Clark Robertson
Chair, Department of Electrical and Computer Engineering

THIS PAGE INTENTIONALLY LEFT BLANK

ABSTRACT

The miniaturization of a sound-detection system is of great interest to applications such as sniper location. Current systems in use are relatively large and do not provide for the unencumbered movement of the warfighter. Inspiration for a smaller MEMS-based sensor is therefore taken from the aural system of the fly Ormia ochracea. The focus of this thesis is the design of an integrated and miniaturized device utilizing commercial-off-the-shelf readout electronics with the biologically inspired sensor. An analysis of previously used techniques is presented along with a novel fully integrated miniaturized design. Specific investigations include integration with external readout electronics, a hybrid discrete component design, and the fully integrated single-package design. Results include successful operation at all levels of integration and a thorough analysis of the performance of the fully integrated design.

THIS PAGE INTENTIONALLY LEFT BLANK

TABLE OF CONTENTS

LIST OF FIGURES

LIST OF TABLES

THIS PAGE INTENTIONALLY LEFT BLANK

LIST OF ACRONYMS AND ABBREVIATIONS

AC	Alternating Current
CF	Feedback Capacitor
CHPRST	Chip Reset
COTS	Commercial-Off-The-Shelf
CS1/CS2	Capacitor Sensor 1/2
CS1IN/CS2IN	Capacitor Sensor In 1/2
CSCOM	Capacitor Sensor Common
dB	Decibel
DC	Direct Current
EEPROM	Electrically Erasable Programmable Read-Only Memory
GUI	Graphical User Interface
HV16	High Voltage (16V)
Hz	Hertz
IAMP	Capacitive Transimpedance Amplifier
IC	Integrated Circuit
K&S	Kulicke & Soffa
KCL	Kirchhoff's Current Law
LDE	Linear Difference Equation
LED	Light Emitting Diode
LPF	Low Pass Filter
MEMS	Microelectromechanical Systems
NC	No Connect
NEFO	Negative Electric Flame Off

Pa	Pascal
PCB	Printed Circuit Board
RMS	Root Mean Square
ROC	Region of Convergence
SC	Switched Capacitor
SCLK	Serial Clock Input
SDATA	Serial Data Input
SNR	Signal to Noise Ratio
SOIC	Small Outline Integrated Circuit
SOIMUMPs	Silicon On Insulator Multi-User MEMS Process
TESTSEL	Test Select
V	Volts
V_{pp}	Volts Peak-to-Peak
V+/VPOS	Positive Rail Voltage
V-/VNEG	Negative Rail Voltage
V2P25	DC Reference Voltage (2.25 Volts)
VDD	Drain Voltage
VLSI	Very Large Scale Integration
VO	Output Voltage
VSS	Source Voltage
WRT	Write Select
ZIF	Zero Insert Force
ZOH	Zero Order Hold

EXECUTIVE SUMMARY

Sniper-location technology is a mainstream product employed by the military utilized around the world. It provides crucial information regarding the origin of enemy fire, which may sometimes be difficult to discern in urban or rural environments.

Several systems currently exist that employ antennae, multiple sensors, or even man-portable devices [1], [2]. These devices are all relatively large and do not provide for the unencumbered movement of the warfighter. Therefore, a need to miniaturize this capability exists. To this end, biological inspiration has been previously drawn from the aural system of the fly Ormia ochracea [3].

In larger animals directional sensitivity is gleaned by sensing differences in pressure at each hearing organ. This is easily accomplished since the separation distance of the hearing organs in larger animals is significant relative to the wavelength of most audible sound. Thus, a pressure difference, large enough to be distinguished by the brain, can be discerned. As the separation between hearing organs becomes smaller the requirement for the animal to process smaller differences in pressure increases [4], [5].

When the hearing organs of insects such as the Ormia ochracea are considered, the wavelength of most audible sound becomes very large relative to the organ separation distance. The fly, therefore, uses a unique hearing organ that can be modeled as a MEMS device. The directional information for this hearing organ lies in the amplitude of oscillations in different resonant modes. Interdigitated comb fingers provide capacitive transduction of sensor movement [5].

This sensor can then be paired with commercial-off-the-shelf (COTS) technology to provide full-readout functionality. In previous work, and in this thesis, the Irvine Sensors MS3110 Universal Capacitive Readout Integrated Circuit (IC) was utilized to this end [6]. This switched-capacitor technology provided excellent resolution for this application. The focus of this thesis lies in the full integration of the readout electronics with the previously designed directional sound sensor.

Three different integrative techniques were detailed in this study. Integration with completely separate and discrete components was first investigated. The readout

electronics were used packaged in both a custom package, termed here a "hybrid design," and with a commercially provided evaluation board. In both cases connections between device components introduced variable parasitic capacitances. These parasitics required that the user continually optimize the readout electronics for consistent performance.

This thesis introduced a third integrative technique where all of the miniaturized components were encapsulated on one device package. Results of this packaging include reduced variability of parasitic capacitances, ease of use, and high angular resolution.

LIST OF REFERENCES

[1] "BBN timeline." [Online]. Available: http://www.bbn.com/timeline/. [Accessed: 23 Feb. 2012].

[2] "Boomerang Warrior-X" [Online]. Available: http://www.bbn.com/products_and_services/boomerang/boomerang_warrior_x. [Accessed: 23 Feb. 2012].

[3] R. N. Miles, D. Robert, and R. R. Hoy, "Mechanically coupled ears for directional hearing in the parasitoid fly Ormia ochracea," *Journal of the Acoustical Society of America*, vol. 98, no. 6, p. 3059, 1995.

[4] M. Touse, J. Sinibaldi, K. Simsek, J. Catterlin, S. Harrison, and G. Karunasiri, "Fabrication of a microelectromechanical directional sound sensor with electronic readout using comb fingers," *Applied Physics Letters*, vol. 96, no. 17, 2010.

[5] M. Touse, "Design, Fabrication, and Characterization of a Microelectromechanical Directional Microphone," Ph.D. dissertation, Dept. Physics, Naval Postgraduate School, Monterey, CA, 2011.

[6] C. W. Lim, "Designing An Electronic Readout For a Directional Micro Electro-Mechanical (MEMS) Sound Sensor," M.S. thesis, Naval Postgraduate School, 2011.

ACKNOWLEDGMENTS

I would first like to thank my predecessors in the study of this sensor. Darren Davis and Mike Touse have both conducted excellent studies from which I was able to glean critical information. In addition, Joe McTighe from Goodrich provided critical insight to make this integration possible. Thank you for your generosity with your time and for providing willing shoulders on which I could stand.

This thesis was in large part made possible by the excellent technical support by Sam Barone and Jay Adeff. Thank you for your expert help in quickly bridging technological gaps that would have otherwise been serious and time-consuming problems.

A debt of gratitude is also owed to Professor Douglas Fouts for agreeing to serve as my co-advisor. I am lucky to have the support of such a dedicated teacher and researcher. It was obvious from the beginning that his first priority has always been students and for that I am deeply grateful.

A very heartfelt thanks is due to my esteemed advisor, Professor Gamani Karunasiri. Thank you for making me a part of your team early on and for the endless hours of patient advice and guidance. Your door was always open and you were always very focused on my success. I can only hope to have such excellent leadership in the future.

I would never have been here if it wasn't for the endless love of my family. Thank you to my parents and brother for your constant encouragement and for providing an amazing upbringing that set the stage for the rest of my life. Your enduring prayers and support have made all the difference.

To my beautiful wife to whom I owe so much, I could never give you enough thanks for everything you have done to make this possible. Thank you for your patient love, encouragement, and support. You have always been the rock on which I stand.

Finally, thank you to Abba Father, the Good Shepherd. Thank you for surrounding me with amazing people and for the diligence to see this through to completion. Without you nothing is possible.

I. INTRODUCTION

A. BACKGROUND

The Microelectromechanical Systems (MEMS) directional microphone investigated in this project originated from the parasitoid fly Ormia ochracea. In larger animals, directional sensitivity is gleaned by sensing differences in pressure fields at each hearing organ. This is easily accomplished since the separation distance of the hearing organs in larger animals is significant relative to the wavelength of most audible sound [1]. The wavelength of sound is given by the well-known formula

$$\lambda = \frac{c}{f} \tag{I.1}$$

where λ is wavelength in meters, c is the speed of sound in meters per second, and f is frequency in hertz.

The key concept is that a pressure difference large enough for the brain to discern must be present across the aural anatomy. As the separation between hearing organs becomes smaller the requirement for the animal to process smaller differences in pressure increases. When the hearing organs of insects such as the Ormia ochracea are considered, the wavelength of most audible sound becomes very large relative to the organ separation distance [1].

Figure 1. The parasitoid fly Ormia Ochracea pictured on a fingernail for scale (From [2]).

1. The Anatomy of the Ormia Ochracea Hearing Organ

The difference in an incident pressure field at each hearing organ of an insect is relatively small, thus new resources must be utilized to glean directional sensitivity. The parasitoid fly Ormia ochracea does this with a novel hearing organ shown in Figure 2 [3], [4].

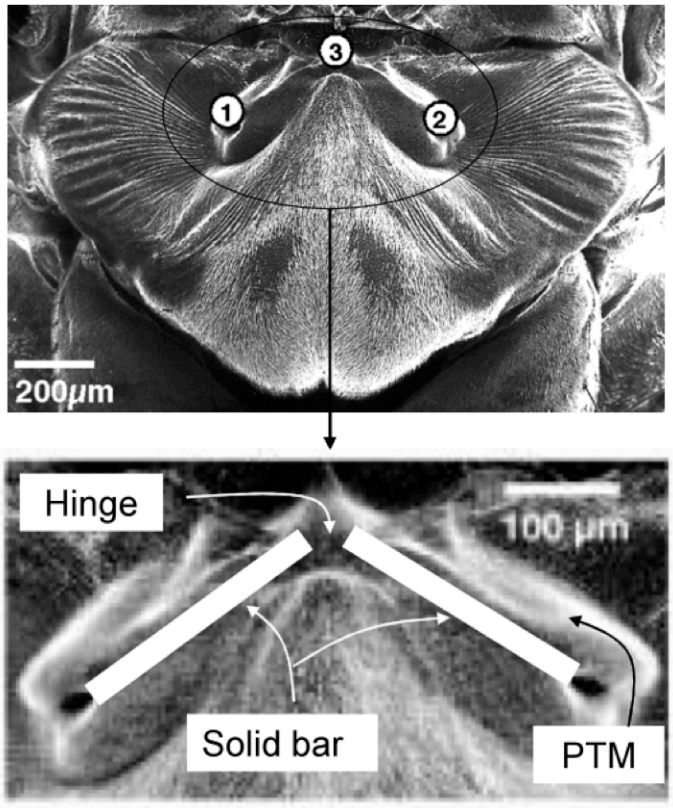

Figure 2. The hearing organ of the Ormia ochracea fly (From [3]).

The hearing organ consists of two tympana mechanically coupled by a circular rod [3]. Under an incident sound wave the organ responds with two main resonant modes as illustrated in Figure 3. The first is the rocking mode and is the most fundamental of all resonant modes. In this mode the device rocks from side to side, each tympana 180 degrees out of phase with the other. The other main resonant mode is the bending mode. In this mode the device tips move upward and downward in phase with each other [3].

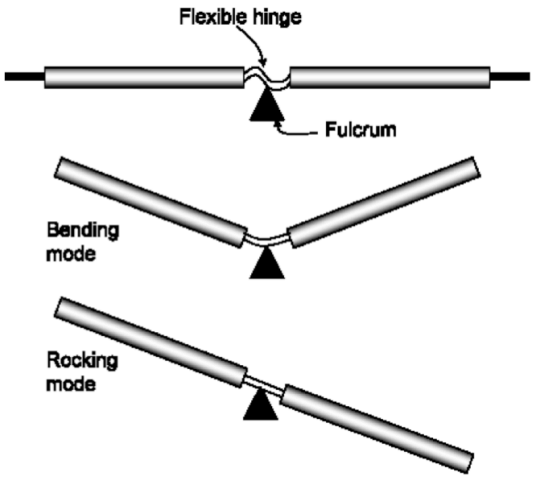

Figure 3. A visual representation of resonant modes of fly's hearing organ (From [3]).

The theoretical frequency response of this simplified mechanical model when excited by sound incident at 45 degrees from normal is presented in Figure 4. Here, the expected response of each side of the device is presented as a separate plot on the same graph. One can note that the interference from the bending mode contributes destructively to the rocking mode on one side of the device while contributing constructively to the other side; this is explained by the aforementioned phase difference. The frequency response clearly shows that resonance at the bending mode induces much larger displacement amplitudes suggesting greater ease of detection.

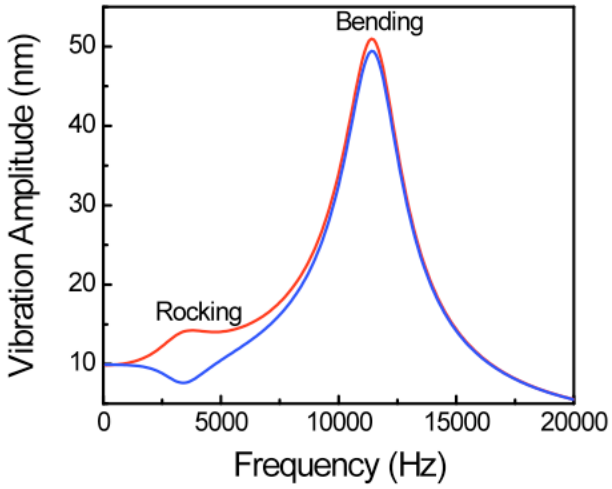

Figure 4. Theoretical frequency response of the fly's hearing organ (From [1]).

The information regarding the direction of the incident sound is found in the amplitude of the response [3], [4].

2. Modeling as a MEMS Device

Touse et al. showed that this organ can be modeled by a simple MEMS device [4]. This device was fabricated using the Silicon on Insulator Multi-User MEMS Process (SOIMUMPs) and was, therefore, subject to the constraints set forth by MEMSCAP Incorporated, a custom-MEMS foundry [5].

The device was connected to the substrate via two legs while the remainder of the device was freestanding as shown in Figure 5. The substrate behind the device was removed to eliminate squeezed-film damping. Each wing had a number of comb fingers that are interdigitated with stationary comb fingers connected to the surrounding substrate. These comb fingers can be thought of as parallel plate capacitors. As each wing moves the capacitance associated with its comb fingers changed as the effective surface area of the parallel plate capacitor changed. A user detected the deflection of the device by sensing the change in capacitance.

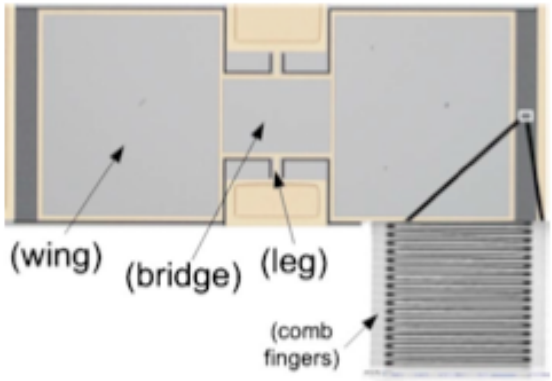

Figure 5. The hearing organ modeled as a MEMS device (From [1], [4]).

In a typical device, each wing was 1 mm^2 while the bridge was 500 µm by 500 µm. The legs were 50 µm by 100 µm. Finally, the comb finger dimensions were chosen to be 100 µm by 2 µm with a separation distance of 2 µm. By minimizing the comb finger width and separation distance while maximizing the comb finger length, the effects

of added mass were minimized while the capacitive effects were maximized. Throughout the design process, the design constraints of the SOIMUMPs fabrication process were followed.

The typical frequency response of this design showed a distinct resonance at both the rocking and bending mode as shown in Figure 6. Further, the amplitude at the bending frequency showed a cosine dependence with the angle of incidence as depicted in Figure 7 [1], [4]. When the angle of incidence was normal to the plane of the device, the magnitude of the response was the largest while an angle of incidence parallel to the substrate gave no response. To understand this phenomenon, consider the case when the angle of incidence was parallel to the substrate. In this case, sound pressure on either side of the wings was nearly the same producing no deflection. The converse is true when the angle of incidence was normal to the organ. Here the phase difference between the sound pressure field on the front and backsides of the wings generated the largest pressure difference resulting in the largest amplitude of oscillation [3].

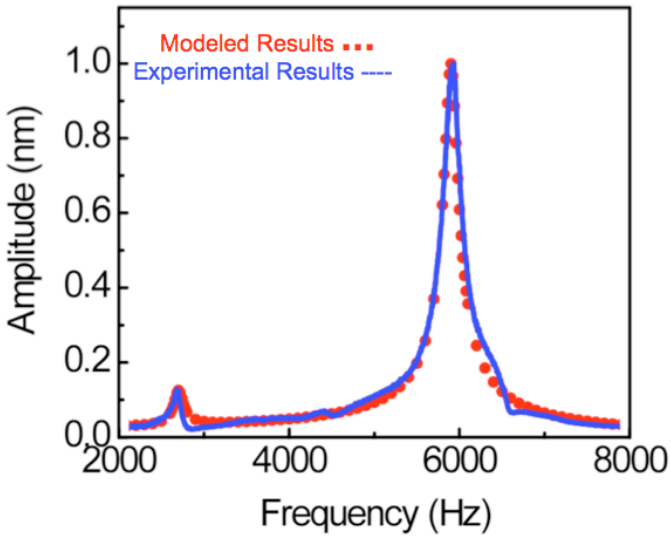

Figure 6. A typical modeled versus experimental frequency response of the MEMS device (After [1], [4]).

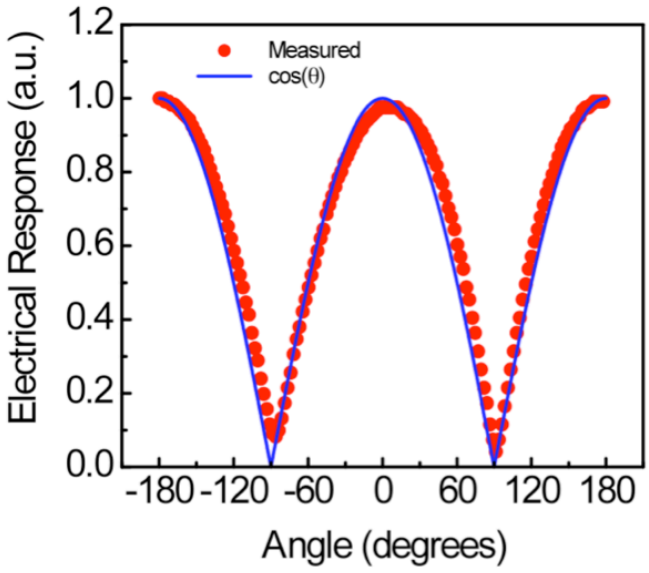

Figure 7. An example of the modeled versus experimental frequency response verifying a cosine dependence on the angle of incidence (From [3]) .

3. Sniper Fire Detection

Several systems currently exist that have employed antennae, multiple sensors, or even man-packable devices. The Boomerang, shown in Figure 8, developed by BBN Technologies, is a vehicle-mounted system employing multiple antennae in order to identify the origin of sniper fire. The Boomerang Warrior-X, shown in Figure 9, is a man-packable device with similar capabilities as the vehicle mounted Boomerang [6], [7].

Figure 8. The vehicle mounted boomerang mounted on a vehicle (From [6]).

Figure 9. The man-packable Boomerang Warrior-X shown being worn on a solider (From [7]).

What these systems all have in common is that they are cumbersome. While they do provide critical information, they also reduce the ability of the warfighter to react. Through MEMS implementation and Integrated Circuit (IC) technology, large steps forward in miniaturization are possible.

B. OBJECTIVE

The purpose of this study was to integrate the MEMS directional sound sensor with readout electronics while keeping the system physical dimensions as small as possible. In this way, the most efficient and least invasive sensor packaging possible for military application was sought. To this end, the Irvine Sensors MS3110 Universal Capacitive Readout IC was used. This IC has previously been used successfully in many high sensitivity capacitive sensing applications [8], [9]. In addition, the small footprint offered by the MS3110 was highly desirable in overall system miniaturization.

C. THESIS ORGANIZATION

An overview of the Irvine Sensors MS3110 Universal Capacitive Readout IC and the steps necessary for successful integration are presented in Chapter II. Special emphasis was placed on troubleshooting and lessons learned so as to prevent their repetition in future work.

The switched-capacitor implementation of the MS3110 is investigated also in Chapter II. To this end, the reader is presented with a comprehensive analysis of the theory of operation. With a better understanding of the inner workings of the MS3110, its proper implementation can be ensured.

Next, the use of the Kulicke & Soffa (K&S) 4525AD wire bonder for MS3110 integration is detailed in Chapter II. Special emphasis was placed on troubleshooting to ensure the results obtained in this study are easily repeatable in the future. The functionality of the various necessary MS3110 connections were also discussed.

Finally, a significant portion of Chapter II was devoted to diagnostic techniques developed for correct MS3110 implementation. This portion of the chapter provides the reader with critical information necessary to efficiently use the MS3110.

Sensor implementation is described and compared at various levels of integration in Chapter III. Integration techniques with discrete components was first investigated then contrasted by an investigation of a fully integrated design with all components encapsulated in a single custom device package.

The original work in Chapter III demonstrated that the fully integrated design was highly desirable relative to the other integrated designs. Successful operation of the fully integrated design was demonstrated through rigorous testing in an anechoic chamber.

THIS PAGE INTENTIONALLY LEFT BLANK

II. MS3110 UNIVERSAL CAPACITIVE READOUT IC

A. OVERVIEW

Three main requirements were central in choosing appropriate processing electronics for this application: small size, fast sampling rate, and the ability to detect capacitance changes in the femto-farad range. The Irvine Sensors MS3110 Universal Capacitive Readout IC was the only commercially available technology found able to meet these needs.

The MS3110 is sufficiently small with dimensions 94.7 mm by 96.1 mm [10]. Further, the MS3110 is capable of sensing capacitive changes down to $4\times10^{-18}\ F/\sqrt{Hz}$ [11]. The MS3110 samples at 100 kHz [11] which is more than adequate to capture signals in the frequency range of interest (2–6 kHz). By the Nyquist theorem a 6 kHz signal would require a sampling frequency of at least 12 kHz.

The MS3110 comes in two forms: a prepackaged 16-pin small outline integrated circuit (SOIC) shown in Figure 10 and a bare die shown in Figure 21. An evaluation board, as shown in Figure 11, was used to allow quick testing of the SOIC without time intensive integration requirements like soldering. The SOIC was inserted into the Zero Insert Force (ZIF) socket on the board and leads were connected to the device, on which the capacitive change would be processed into an output waveform.

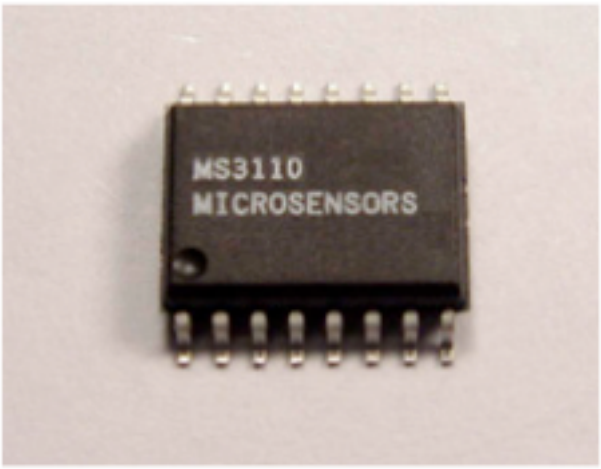

Figure 10. Here a close up view of the MS3110 16-Pin SOIC is presented (From [11]).

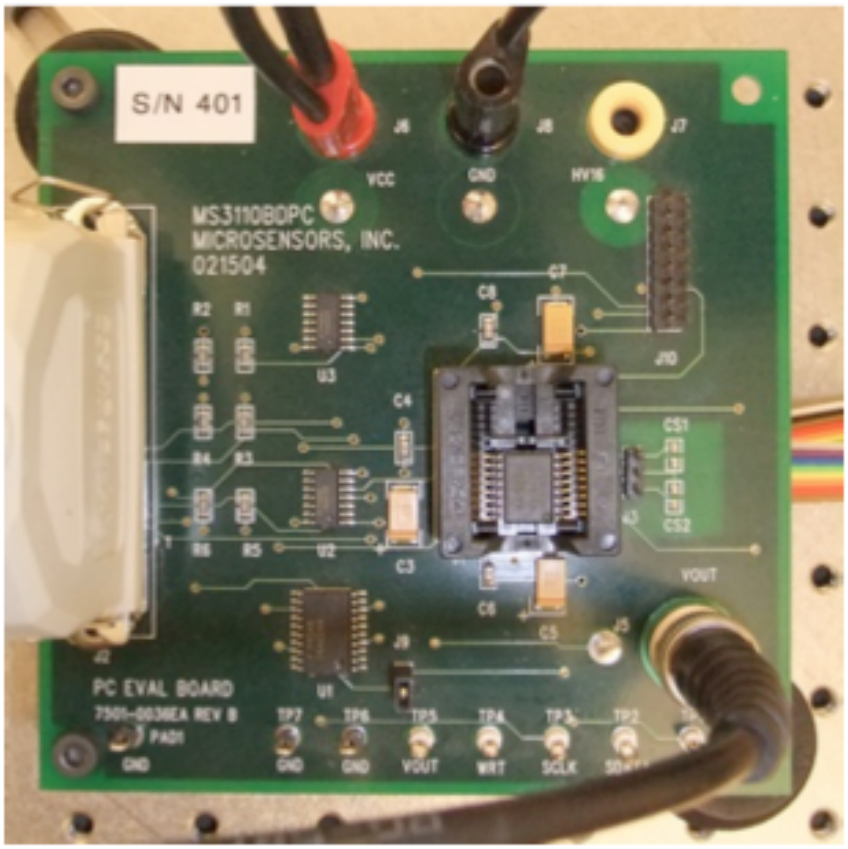

Figure 11. Here the interconnects of the MS3110 evaluation board are shown (From [12]).

B. THEORY OF OPERATION

There are three main components to the MS3110. They are a Capacitive Transimpedance Amplifier (IAMP), a low-pass filter, and an output buffer. The functionality of the MS3110 can best be understood by first considering the IAMP. This stage consists of a capacitor bridge followed by an amplifier. The bridge was driven by a 100 kHz square wave that oscillates between ground and 2.25V. The bridge was thus an implementation of switched capacitor (SC) technology.

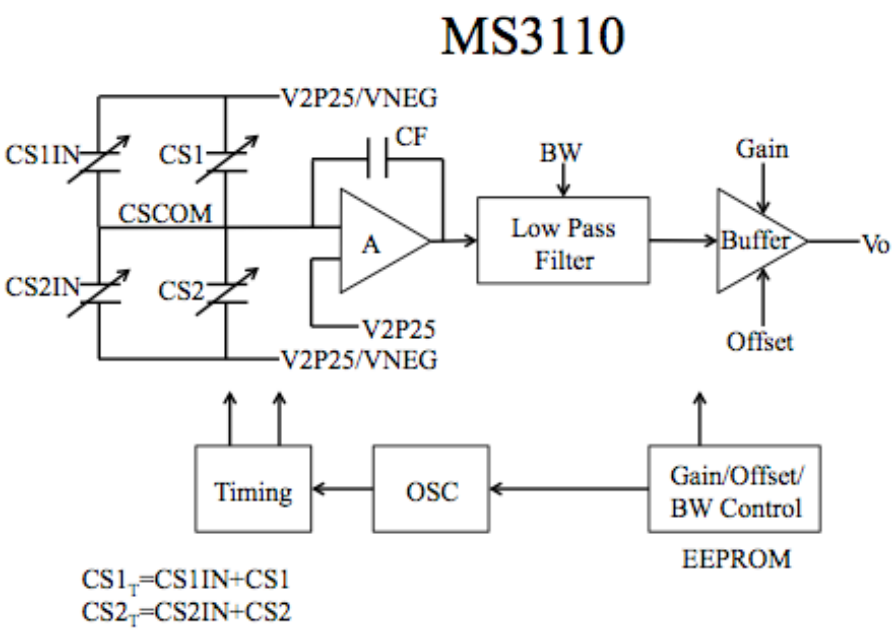

Figure 12. The MS3110 is presented in block diagram form (After [11]).

1. The Switched Capacitor as a Resistor

To best understand the implementation of the capacitor bridge in the MS3110 IAMP, a brief introduction to SC technology is appropriate. SC technology is popular in modern very large scale integration (VLSI) circuits since capacitors are much easier to fabricate reliably than resistors.

To begin, recall that current is charge per unit time and Kirchhoff's Current Law (KCL) are given by

$$i = \frac{dq}{dt} \tag{II.1}$$

$$\sum_n i_{in,n} = \sum_n i_{out,n} \tag{II.2}$$

where n spans the set of current branches at a given node, $i_{u,v}$ is current in the u direction at node v, q is charge, and t is time. These relationships can be extended to discrete time in the form of a charge conservation concept over the set of capacitors M

$$\Delta q[k] = \sum_M q_{in,M}[k] - \sum_M q_{out,M}[k] \tag{II.3}$$

where $q_{u,v}$ is charge in the u direction over the set of capacitors v, and k is a sampled interval of time.

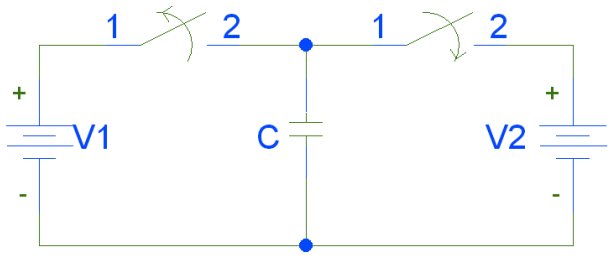

Figure 13. This simple SC circuit models a resistor (After [13]).

Consider the simple SC circuit, shown in Figure 13, with two voltage sources connected in parallel, via independent switches, with a capacitor. The switches are 180 degrees out of phase with each other with a period of T seconds. As switch one is closed and switch two is opened the charge, q, held by the capacitor is given by

$$q = CV_1, \tag{II.4}$$

where C is the capacitance in farads and V_1 is the voltage across the first voltage source. If switch two is closed and switch one is opened the charge on the capacitor is given by

$$q' = CV_2, \tag{II.5}$$

where q' is the charge held in the capacitor and V_2 is the voltage across the second voltage source. Thus, the total charge moved can be described by

$$\Delta q = q - q' = C\left(V_1 - V_2\right). \tag{II.6}$$

Because current is described as charge moved per unit time we get

$$I = \frac{\Delta q}{T} = \frac{C\left(V_1 - V_2\right)}{T}. \tag{II.7}$$

As this process is repeated, charge is constantly moved at a rate given by (II.7). Finally, by rearranging Ohm's Law we find the equivalent resistance as

$$R = \frac{\Delta v}{I} = \frac{T}{C}. \tag{II.8}$$

Thus, through using SC technology a capacitor can be modeled as a resistor with resistance T/C[13].

2. Capacitive Transimpedance Amplifier Analysis

From above we have seen how a capacitor can be modeled as a resistor in a SC network. This idea will be used to simplify the IAMP operation analysis.

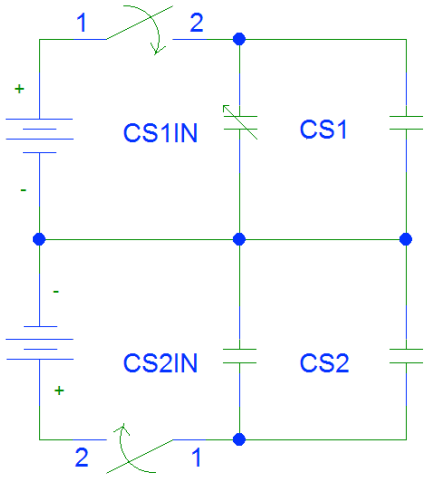

Figure 14. Here a circuit diagram of IAMP capacitor bridge is presented (After [12]).

Note that the capacitors CS1 and CS2 in Figure 14 are internal to the MS3110 while the capacitors CS1IN and CS2IN reside on the MEMS directional sensor. CS1IN and CS2IN are interchangeable but for the purposes of this discussion let CS1IN represent the capacitance of the interdigitated comb fingers on the perimeter of the MEMS wings. This capacitance varied as the wings moved. CS2IN is a capacitor bank on the MEMS sensor that was closely matched to the stationary value of CS1IN. CS2IN was a fixed value and did not change throughout the device operation. Finally, we can combine the capacitors in parallel

$$CS1_T = CS1 + CS1IN \tag{II.9}$$

$$CS2_T = CS2 + CS2IN \tag{II.10}$$

to yield the simplified schematic in Figure 15.

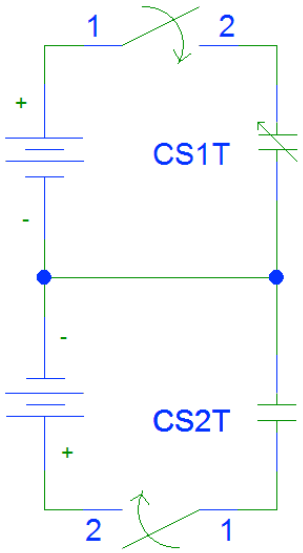

Figure 15. Here a simplified schematic of the bridge is presented.

Here, $CS1_T$ varied with the displacement of the MEMS wings while $CS2_T$ remained constant. Using a conceptual understanding of SC technology the following equivalencies can be made

$$R_1 = \frac{T}{CS1_T} \tag{II.11}$$

$$R_2 = \frac{T}{CS2_T}. \tag{II.12}$$

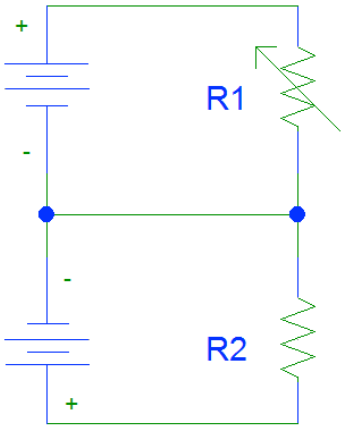

Figure 16. Here the switched capacitors of the IAMP circuit are shown as equivalent resistors.

As R_1 varied the voltage divider stipulates that the signal value at the amplifier input also varied. This signal was then amplified before the next stage of the MS3110.

This amplifier is in an inverting configuration resulting in a signal at the amplifier output that is 180 degrees out of phase with the input signal. The overall gain of the amplifier was largely a function of, and inversely proportional to, the feedback capacitor CF as shown in Figure 12. In other words, the larger the feedback capacitor value the smaller the output and vice versa. However, lowering the feedback capacitance too far risked saturating the output of the amplifier and clipping the output signal or introducing harmonic distortion into the signal. Touse has previously established that a value of 1 pF is generally a reasonable compromise between signal strength and distortion [1]. The very low changes in capacitance in this application were generally not a concern.

3. Low Pass Filter and Output Buffer Analysis

The next main component in the MS3110 was a low pass filter (LPF) that consists of two sub-components: a zero order hold (ZOH) circuit and a two-pole reconstruction LPF. The main function of this component was to take the digital output of the IAMP and convert it to an analog signal [11].

The ZOH circuit takes a discrete time input and interpolates between samples with a zero-order polynomial. The resulting output of the ZOH was a step function with a significant high frequency component. These high frequencies were then eliminated via the two-pole LPF.

The LPF 3dB frequency was piecewise adjustable from 500 Hz to 8 kHz with nine possible discrete values within these extrema. It should also be noted that the bandwidth selection error could be as high as +/- 21% [11]. The relative simplicity of this LPF resulted in a long transition between pass and stop bands with a roll-off of 40 dB/decade and thus could not be neglected.

The 3dB frequency for this filter dramatically affected the output of the MS3110. Choosing a low frequency provided excellent harmonic rejection but if the frequency of

interest is above the cut-off frequency it suffered attenuation. Conversely, if a high 3 dB frequency was used the frequency of interest suffered less attenuation, but the same was true of the unwanted harmonics.

The output buffer was the last main component in the MS3110. The output buffer provided three main functional benefits. First, the buffer provided low output impedance. This is highly desirable when connecting follow-on electronics as the lower the output impedance the more the device will serve as an ideal source. Second, the buffer provided a final gain to boost the signal strength. This gain is nominally at 4 V/V and is adjustable to 8 V/V. An additional fine gain trim is available and piecewise adjustable from -15% to +15% in 2.4 mV/V steps. The fine gain trim was accurate to +/- 300 mV/V. Finally, a DC offset adjustment was available to correct any intrinsic transistor mismatch in the amplifier. This adjustment was also piecewise adjustable within the range +/- 100 mV in 6.25mV steps. Care was taken when providing output buffer adjustments so as to not saturate the transistor and clip the output waveform [11].

The output of the MS3110 [11] is

$$V_O = Gain \cdot V_{2P25} \cdot 1.14 \cdot \frac{CS2_T - CS1_T}{CF} + V_{REF} \cdot \tag{II.13}$$

C. MS3110 WIRE BONDING

In this study, wire bonding of the readout electronic die was performed using a Kulicke & Soffa (K&S) 4525AD wire bonder, shown in Figure 17. Several connections were required to ensure proper operation of the MS3110 with the MEMS directional sound sensor. In the process of this study, deviations from the equipment documentation were required in order to affect proper bonding. This section provides a summary of the bonding process along with a discussion of the aforementioned deviation.

Figure 17. Here the K&S 4525AD wire bonder is shown.

1. Wire Bonder Setup and Use

The component to be wire bonded was snugly inserted into the metal heating element as shown in Figure 18. A spring-loaded socket was available to this end and the socket width was manually adjusted with a screwdriver for proper fit.

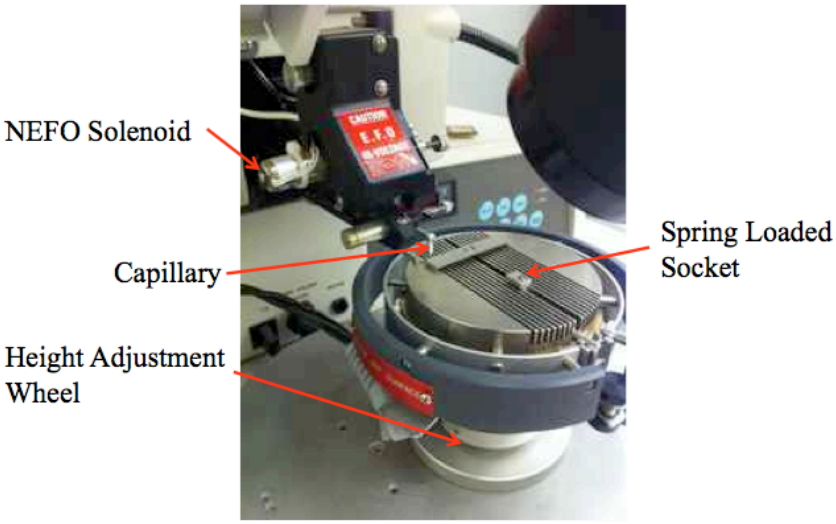

Figure 18. A close up of the wire bonder working assembly is depicted with various components annotated.

The wire bonder was turned on via the red power switch near the screen shown in Figure 19. Nothing was under the wire bonder as the wire bonder sometimes moved downward during start up and could cause damage to anything directly underneath the capillary. The wire bonder was always allowed to heat to approximately $120°C$ before any bonds were attempted. Once this temperature was reached care was taken when moving the heating element and tweezers were always used when manipulating the die and package to prevent personal injury.

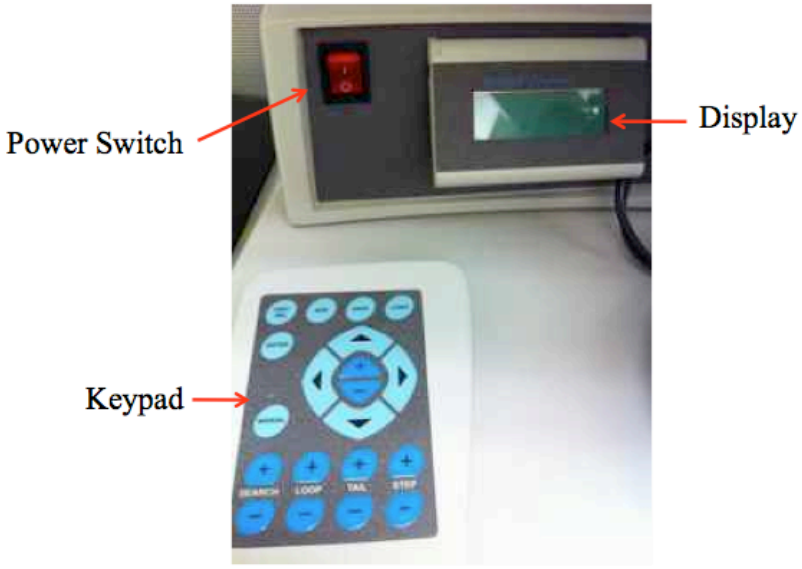

Figure 19. The wire bonder left control panel is shown with various components annotated.

It was important for the device to heat at the same rate as the heating element. This prevented heat shock to the device that might have otherwise caused damage or brittle and break adhesives. If multiple devices were to be wire bonded, the wire bonder was allowed to completely cool before inserting and heating another device. Also, the short amount of time the MS3110 and the MEMS device were subject to high temperatures did not seem to carry any adverse effects.

It took several minutes for the wire bonder to heat to operating temperature and this time was used to adjust the settings. When the wire bonder was first powered on,

password mode was disabled when prompted via the down arrow and then enter. A new screen with a '1' highlighted and several settings followed. The wire bonder was designed to be used in two phases. During the first phase the first bond was made to the MS3110 but the wire filament remained attached to the wire bonder capillary. During the second phase the second bond was made to the device package and the wire filament was cut and reset for the next series of bonds. The bonds were made to different materials at different heights; therefore, separate settings were assigned to each phase of the bonding process. Settings were changed by scrolling through the options with the up and down arrow and adjustments were made with the + or – button. Scrolling to the bottom of the first screen and pushing the down arrow accessed a second screen to adjust the values for the second bond. Scrolling to the bottom of the second screen and pushing the down arrow accessed a third screen that was not needed for this application. Finally, scrolling to the bottom of the third screen and pushing the down arrow returned the wire bonder to the first screen.

Davis [14] previously established ideal settings (see Table 1) for wire bonding between the MS3110 and the gold contacts of commercially available packages.

Table 1. Optimal wire bonder settings for bonding the MS3110 to the custom package.

	1st Bond	2nd Bond
Power	1.8	2.07
Time	5	5
Force	1.8	1.8
Loop	N/A	4
Tail	N/A	4.5
Ball	N/A	4

Adjustments to ‘Loop’ and ‘Tail’ were done via dedicated + and – buttons provided as separate controls. ‘Ball’ was adjusted via the right arrow when the text immediately to the left of ‘Ball’ was highlighted. ‘Search Height’ was a function of the heating element height and the height of the subject to be wire bonded and was determined empirically during each use.

The wire bonder was first switched to manual mode by depressing the ‘manual’ button on the controls before using it in the more desirable semi-automatic mode. By first cycling the wire bonder through manual mode, proper operation in semi-automatic mode was assured. Once the wire bonder was in manual mode a green light emitting diode (LED) next to the manual button illuminated verifying this mode of operation. The heating element was then moved so the device was not underneath the wire bonder and the black thumb button on the mouse, shown in Figure 20, was depressed and released. This manually engaged the wire bonder to make the first bond although no actual bond was desired yet. This was done once more to engage the wire bonder to make the second bond, again with no actual bond made. Finally, the manual button was pressed a second time to exit manual mode. It was verified that the wire bonder was no longer in manual mode by observing that the aforementioned LED no longer illuminated.

Figure 20. The wire bonder right control panel is shown here with various components depicted.

The last step before using the wire bonder was to set the search height for both bonds. This was done by first raising search height number 1 to a height of 1.50. For proper operation it was important to make the first bond to the MS3110 pad and not the packaging. Next, with the device to be bonded near but not directly underneath the capillary, the left mouse button was depressed and held. The capillary moved downward but did not yet make the first bond. The dedicated + and – buttons on the control panel were then used to adjust the height of the bonder until it was just above the MS3110 pad to be bonded. Once the proper height was achieved, the left mouse button was released and the wire bonder made the first bond to the die.

Next, the search height number 2 was raised to a value of 1.50 with the package bond pad near but not directly underneath the capillary. The heating element was moved slightly to ensure that the MS3110 was also not directly underneath the capillary thus avoiding any incidental contact of the capillary with the die or package. Again, the left mouse button was depressed and held. After the button was depressed the capillary moved downward but did not make the second bond. For proper wire bonder operation it was important to make the second bond to the package and not the MS3110. Care was taken to slowly move the capillary over the packaging pad. The capillary height was then lowered until the capillary was actually touching the pad. The left mouse button was released and the wire bonder completed the bond, automatically removed any excess filament, and reset for the next bond. Each search height was raised slightly before making each bond and the above process was repeated. By doing this, damage to the die, package, or the wire bonder was prevented.

2. Wire Bonder Troubleshooting

During the course of wire bonding, malfunctions of the K&S 4525AD were common. This section illustrates corrective techniques taken and expands on and emphasizes those provided in the wire bonder documentation [15].

a. The Wire Bonder Will Not Engage

A common mode of malfunction was a wire bonder that was completely unresponsive. This happened frequently while making multiple bonds. Often this problem

resulted from the filament ball protruding from the capillary being accidentally damaged during bonding. This was verified by checking the controls near the temperature gauge. If a yellow LED labeled ‘open’ was lit, the filament needed rethreading through the capillary (see Section c).

b. The Wire Bonder Will Move but Not Make Bonds

While making multiple bonds another mode of malfunction was the outward appearance of proper operation, but no actual bonds being made. Like the previous mode of malfunction, this was usually the result of damage to the filament during operation. This malfunction was verified by using the microscope to check if there is a ball at the end of the filament. If not, it needed to be rethreaded through the capillary (see Section c). Also, the likelihood of this malfunction was increased if improper settings were used, thus the settings on the wire bonder were also verified as matching those provided. The settings provided in Table 1 are ideal for bonding to the MS3110 pad to the packaging and may not be applicable to different materials.

c. The Capillary Must Be Rethreaded

If a malfunction caused damage to the filament it typically needed to be rethreaded. First, to accomplish this, the ‘Open Clamp’ button on the right side control panel was depressed. A corresponding LED lit to confirm an open clamp. Tweezers were then used to take hold of the filament above the capillary yet below the clamp. The filament was then gently moved downward through the capillary. If the filament did not move through the capillary it was inferred that the capillary was clogged. The filament was first removed from the capillary with tweezers to unclog it. The capillary was then cleaned by plunging a cleaning wire through the opening. Next, ensuring the filament remained in the clamp, it was inserted into the capillary and slowly moved downward until it protruded out the other end. Once the filament protruded out of the bottom of the capillary, the clamp was closed by pressing the ‘Open Clamp’ button a second time. The LED then turned off confirming the clamp was closed. Finally, the button in the upper left of the wire bonder was used to move the negative electric flame off (NEFO) solenoid near, but not touching, the protruding filament. The ‘Manual Spark’ button was then

depressed in an attempt to ball the end of the filament. This button sometimes needed to be pressed several times in order to create a successful ball. Once this was done the open LED turned off confirming a proper ball. The wire bonder was then ready for further use.

3. MS3110 Connections

The MS3110 has several connections that were required in order to ensure proper operation [10]. The pre-packaged SOIC connections are listed in [10] and were straightforward. The ZIF socket of the evaluation board provided user-friendly access to the functionality of the chip with the only requirement that the MS3110 was properly oriented and seated in the ZIF socket.

The bare die, shown in Figure 21, form of the MS3110 was approached slightly differently in order to ensure proper operation. **The MS3110 is a mixed-mode device and required a digital and analog ground and a digital and analog power supply**. Reference [10] lists three pads as VNEG and one pad each as VDD and VSS. Any of the three VNEG pads may be used for ground. It was critical that both VDD and VPOS were connected to the positive rail voltage (5V) and VSS and VNEG were connected to a common ground. If any of these pads are left unconnected the MS3110 did not function properly. The remainder of the pads were connected as described in reference [10].

Finally, when a modular power supply and coaxial cable readout were used as described in Chapter III, one of the unused VNEG pads was connected to a second pin designated for ground. This was to provide a common ground for both the coaxial-cable shielding and the modular power supply.

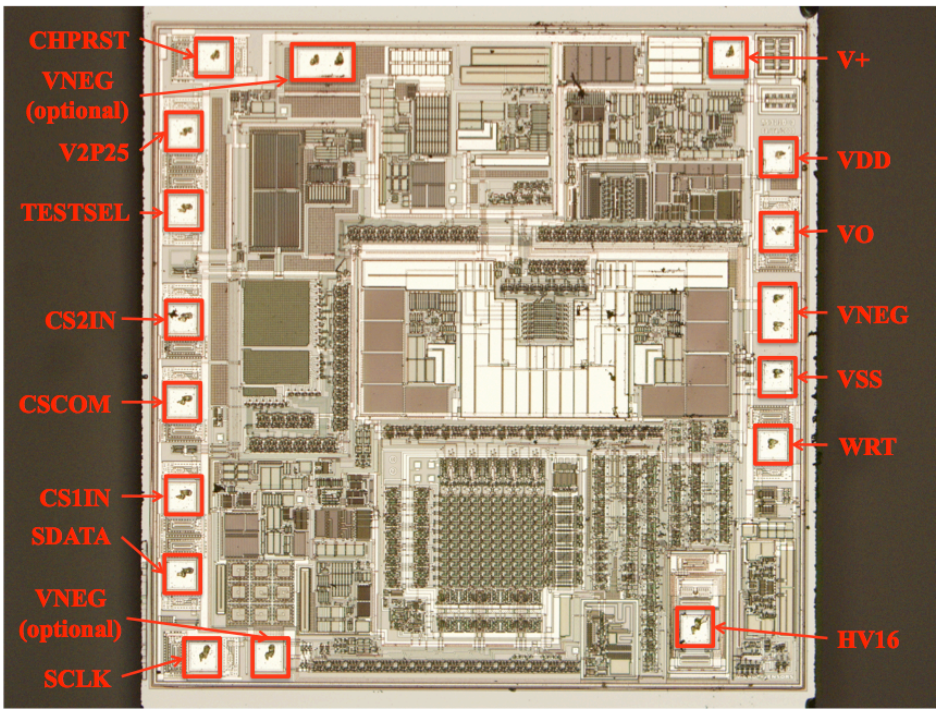

Figure 21. A microscope image of the MS3110 and pin out are presented.

D. MS3110 DIAGNOSTICS

Setting up and biasing the MS3110 was not a trivial task. The MS3110 offers a wide variety of ports to verify correct operation. Operational diagnostics is a valuable prelude to the experimental process and results.

1. Internal Oscillator

The MS3110 was driven by an internal 100 kHz square wave shown in Figure 22. The existence of the oscillator waveform was an excellent indicator of correct operation. A good indicator that the MS3110 was not powered properly was if the oscillator waveform could not be observed. The square wave was observed between CS1 and ground or CS2 and ground.

The oscillator was powered by the 5 V power supply and a square wave was observable immediately after powering the MS3110 and before any other operation was taken. The waveform was nominally 2.25 V_{pp} and 100 kHz. The frequency of the square

wave could be adjusted with the MS3110 software via the oscillator trim. For correct operation the oscillator frequency was within 5 kHz of 100 kHz [16].

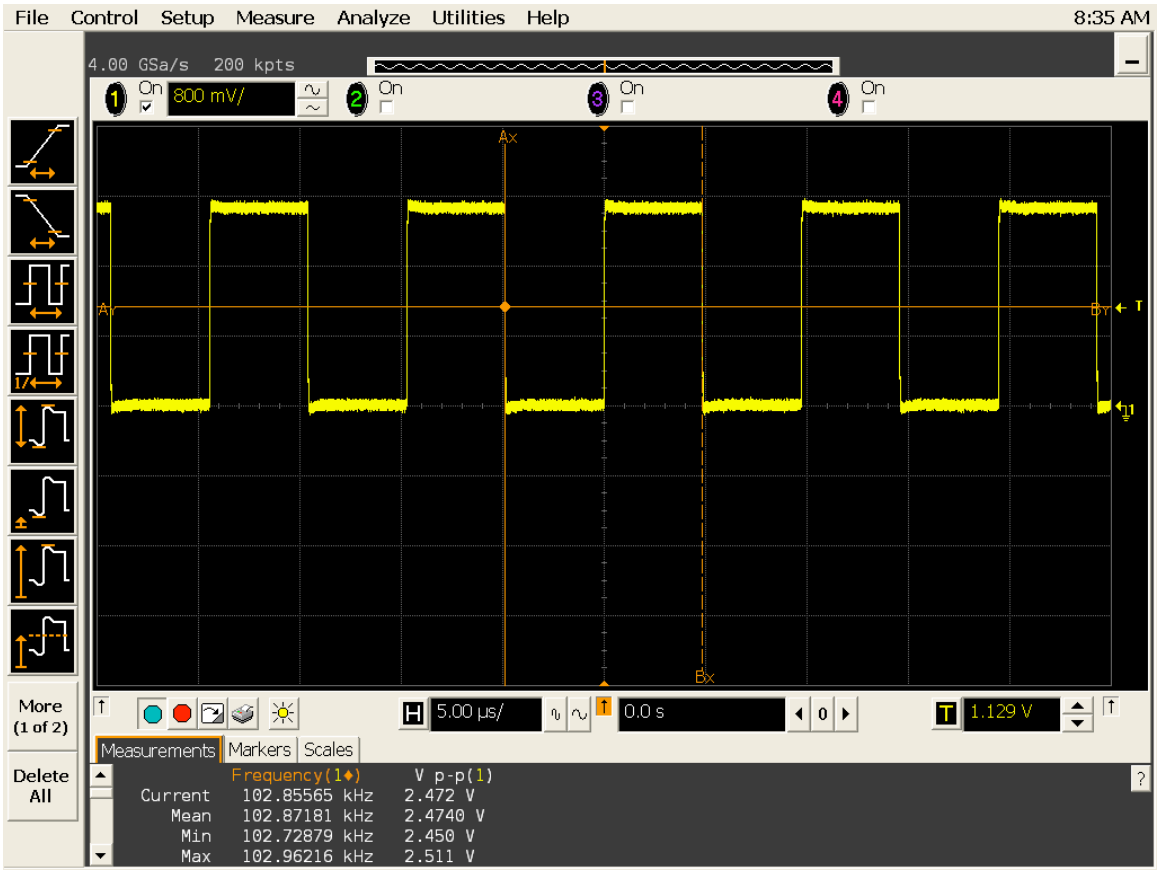

Figure 22. The oscillator waveform measured between CS1 or CS2 and ground is shown here in yellow.

2. Parasitic Capacitances

Parasitic capacitances, at times, played a significant role in the balancing of the bridge in Figure 14. Sometimes the parasitic capacitances were so large that the bridge could not be balanced. The primary symptom of this problem was a device that was powered properly but the output DC voltage could not be adjusted through the full dynamic range or would not move at all. This was a typical situation when the leads attaching the MS3110 to the sensor were long. Manually manipulating the leads from the MS3110 to the MEMS sensor sometimes solved this problem. Adjusting the lead position

randomly caused the output waveform to 'jump' as fingers introduced more parasitic capacitance. Enough manipulation always yielded a system that could be balanced.

3. Verification by Laser Vibrometer

At times the MS3110 was properly working but the sensor was not. Verification of sensor operation was done with a laser vibrometer. To test this, the device was excited at the bending-mode resonant frequency and the displacement was measured. Although this test verified operation of the sensor, the frequency response of the device was also verified. For maximum response the sensor was always be excited at its bending-mode resonant frequency. Use of the vibrometer was detailed by Touse in reference [1].

4. Ambient Light

The MS3110 was tested extensively with and without a light-resistant package. No differences in operation or internal resistances were noted. This suggests that exposing the MS3110 to ambient light has no effect on operation.

5. Common Problems Associated With Setup

a. Spontaneous Reset

Often, while operating the MS3110 on settings previously written to the volatile registers, the output voltage dropped to zero. This was a symptom of a spontaneous reset of the MS3110 and was remedied by issuing a chip reset then rewriting to the volatile registers. Often this reset was the result of other software running on the same computer as the MS3110 software. Specifically, the laser-vibrometer software seemed to trigger a reset of the volatile registers.

b. Proper Connections

It was sometimes difficult to ensure that proper connections were made. Care was taken specifically when installing the leads on the J3 socket of the evaluation board, when connecting the soldered leads to the MS3110, and when connecting the soldered leads to the fully integrated MS3110 and sensor as these connections required fastidious attention for proper setup.

c. Write Jump

When writing to the MS3110 using the software, the DC or alternating current (AC) coupled output waveform noticeably jumped. If this did not happen it was a good indication that the MS3110 was not powered or functioning properly and settings were not written to the volatile registers. Various diagnostic steps outlined in section 5 of this study were taken to find the source of this problem.

d. Chip Reset

Often, issuing a chip reset solved seemingly irresolvable problems. This was the first step taken when diagnosing a problem.

e. Oscilloscope Setup

Oscilloscope settings were frequently checked while troubleshooting. Specifically, care was taken to ensure the oscilloscope was always properly AC coupled. The oscilloscope must be DC coupled to balance the capacitors and thus the oscilloscope was frequently left in this mode as opposed to being AC coupled for proper sensing of capacitance.

f. Soldered Leads

Due to the nature of several setup configurations, some soldered leads were routinely left unconnected. It was crucial for proper operation that these leads did not touch each other or any other conducting surface.

g. Wire Bonding

A microscope was used to ensure the integrity and location of each of the wire bonds made to the package. The package pads were mapped to pins through the use of a multimeter. Very low impedances verified mapping from a pad to a pin and infinite impedance verified a lack of an electrical connection between a pad and a pin.

THIS PAGE INTENTIONALLY LEFT BLANK

III. SENSOR INTEGRATION AND TESTING

Figure 23. Experimental setup overview.

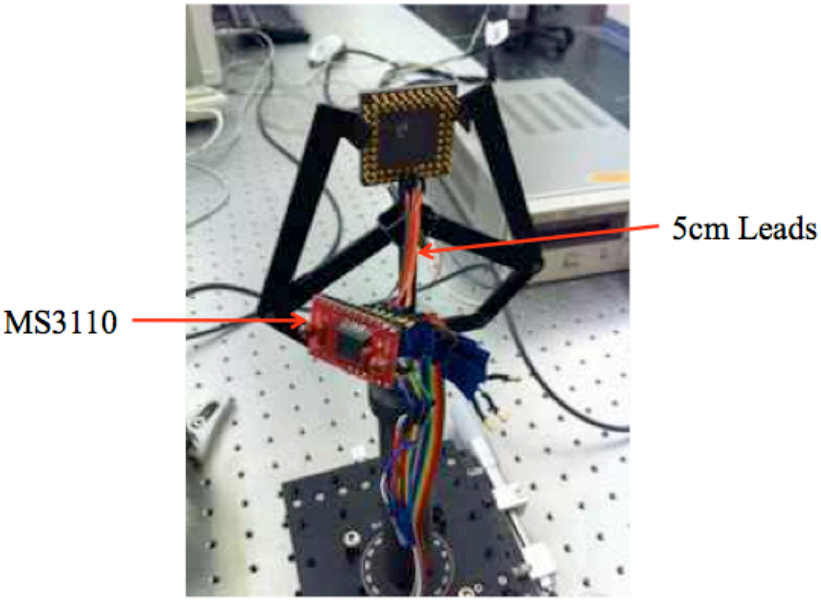

Figure 24. Packaged chip connected to the MEMS sensor using short leads.

A. INTEGRATION WITH HYBRID DESIGN

The goal of this part of the study was to verify the hybrid-integration method reported by Lim [12]. In this method, the prepackaged SOIC was soldered to a printed circuit board (PCB) along with the recommended external components described subsequently. The advantage of this type of packaging was a semi-miniaturized discrete stand-alone capability. Theoretically, the MEMS device could be mounted with this setup and used as a single integrated system although this had not yet been demonstrated. The MEMS directional microphone used was a generation 7 sensor with a bending-mode resonant frequency of 3.5 kHz mounted in a generic package. A hole was drilled in the ceramic package to allow the pressure field to properly affect both sides of the device and to prevent squeeze-film damping.

A minimum of external components was required to optimize the performance of the MS3110. It was recommended that a $0.1\,\mu F$ capacitor and a $10\,\mu F$ capacitor be installed in parallel with the V2P25 pin and the positive-power supply (see Figures 24 and 25) to filter unwanted frequencies.

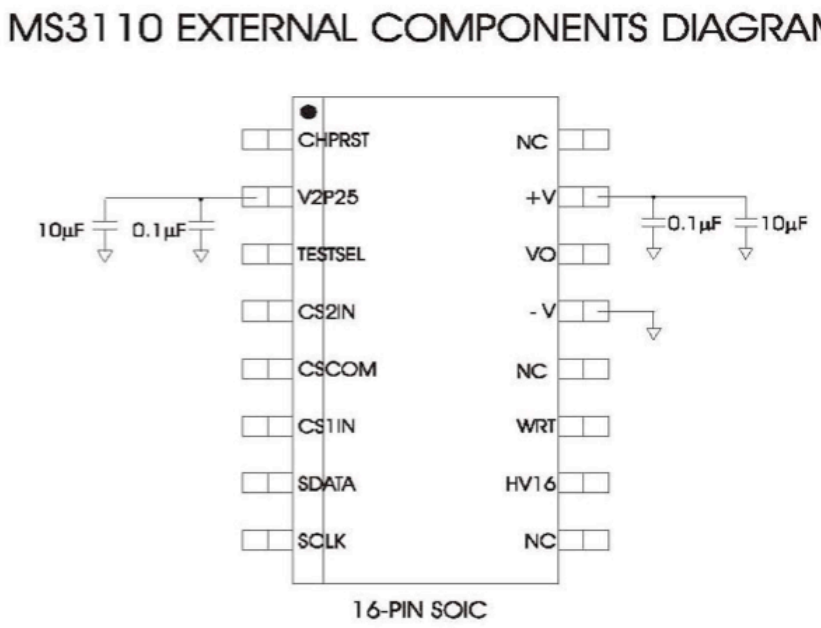

Figure 25. MS3110 IC is presented here with external capacitors.

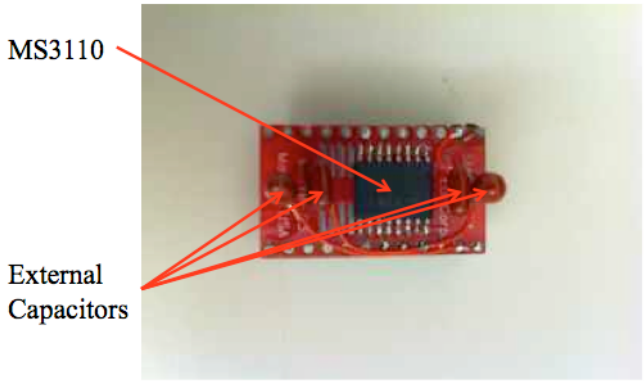

Figure 26. A hybrid MS3110 package with external capacitors attached to the circuit board is shown here.

In this setup, it was necessary to solder wires to the bottom of an evaluation board (see Figure 27) in order to access all of the pins of the MS3110, which the standard J10 cable did not offer.

Figure 27. The soldered underside of the MS3110 evaluation board is shown here.

The solders were made, previous to this study, to the reverse of the ZIF socket. This enabled a packaged MS3110 to be programmed via the evaluation board without it actually being inserted in the ZIF socket (see Figure 29). The soldered leads were then connected to the hybrid PCB that was then connected via 5 cm leads to the MEMS sensor as shown in Figure 28.

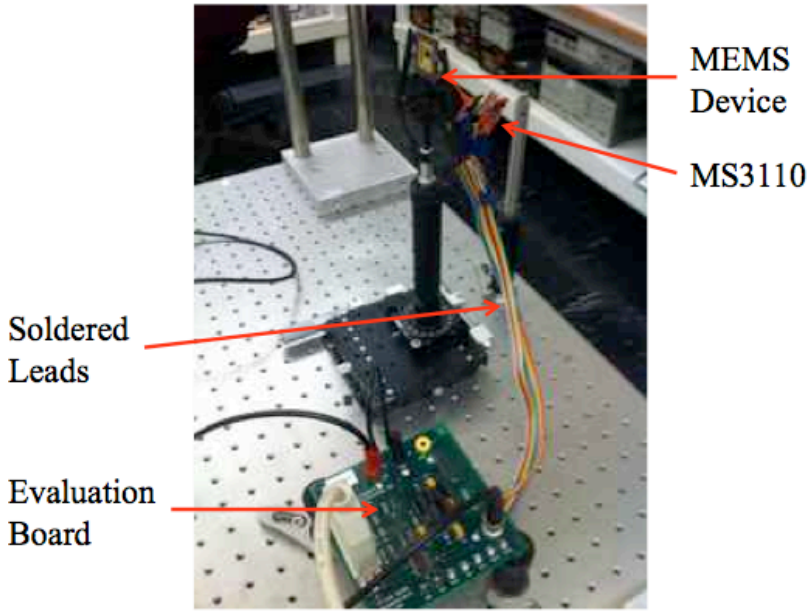

Figure 28. The full hybrid setup is shown here; note the packaged chip with the evaluation board.

The experiment was started by powering the evaluation board (see Figures 27 and 28). At this point V2P25, measured at test point 1 on the board, was 2.25 V +/- 10 mV as required for proper operation. If this value was not observed, but was very close to the required value it was adjusted using the voltage reference trim on the MS3110 software. If it was observed to not be close to the required value, diagnostic steps outlined in Section II.D.5 were taken.

The internal capacitors were then balanced to provide a 2.25 V DC voltage at the output. To do this, the oscilloscope was first set to DC coupling to monitor the DC value of the MS3110 output. A CF value of 0.531 pF was chosen in this portion of the study in order to maximize the output waveform. When both CS1 and CS2 were set to 0 pF the output voltage read the maximum value of 5 V. When both CS1 and CS2 were set to their maximum value the output voltage read the minimum value of 0 V. In order to standardize this portion of the study, CS2 was always set to 1.083 pF. As the value CS1 was typically in the lower regions of its dynamic range, efficient balancing started with CS1 at 0 pF. CS1 was then increased until the output voltage fell below 5 V. In this way, the balanced value of CS1 was found using an iterative bracketing method. The

remaining values, such as gain and the cutoff frequency of the LPF, were left at nominal values.

It should be noted that for the same setup, the value of CS1 when balanced differed every time the system was balanced. This was because of different parasitic capacitances due to different lead configurations and other environmental conditions. Therefore, balancing a setup established a likely range for the next setup, but not an exact value.

The output voltage of the MS3110 was tapped at the Vout terminal on the evaluation board and connected to an Agilent Infinium DSO8064A oscilloscope. The board was powered with a 5 V Hewlett Packard E3615A DC Power Supply connected to the J6 banana jack and grounded via the J8 jack. The J9 jumper was bridged and the computer was connected to the board via the parallel-port connector.

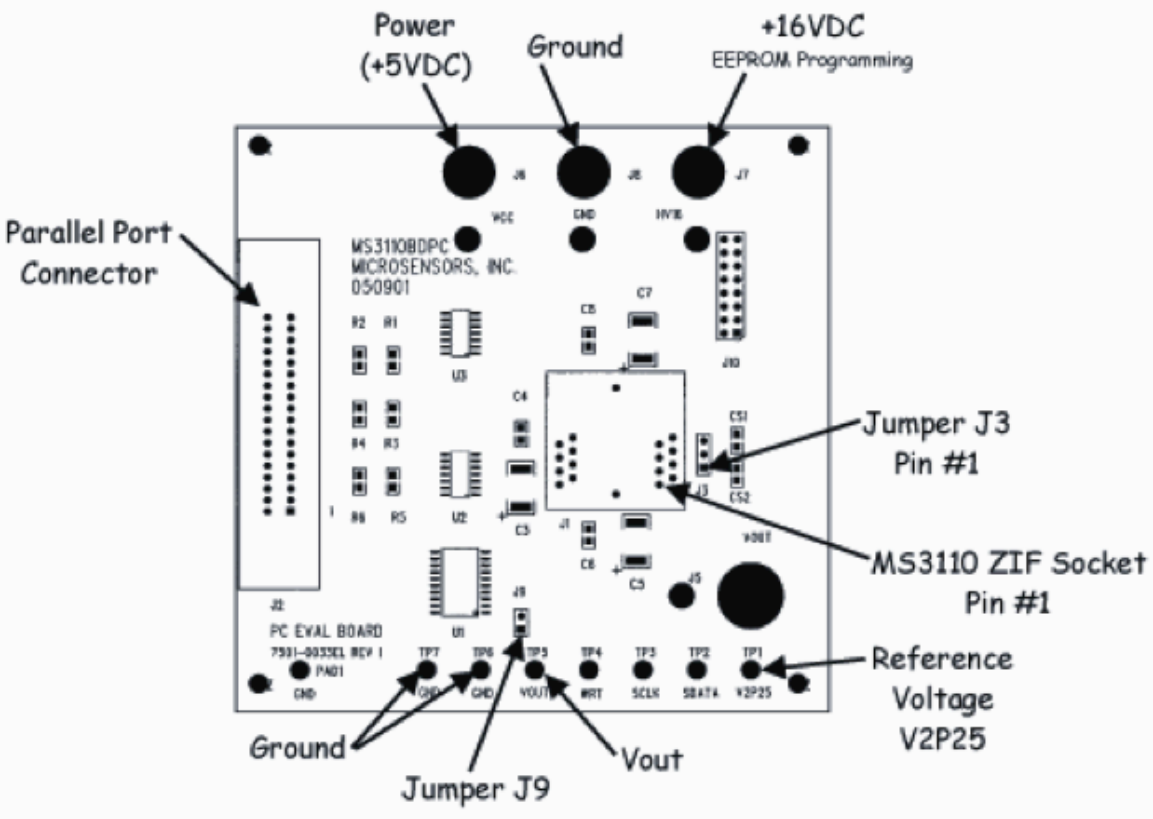

Figure 29. The evaluation board layout and topology is presented here (From [11]).

The oscilloscope was then set to AC coupling. Typically, a range of approximately 50 mV/division along the ordinate and 200 μs/division along the abscissa allowed for ideal viewing of the MS3110 output.

The speaker was offset by 20° and the MEMS device was excited by monochromatic sound at its bending-mode resonant frequency via a Hewlett Packard 3314A function generator. The signal strength of the function generator was set to 79.3 mV throughout this study unless otherwise noted.

An output signal was successfully generated and recorded to be about 75 mV_{pp}. This signal was sensitive to the angle of incidence and attenuated as the speaker was rotated away from normal and vice versa. A notable observation was significant harmonic distortion and corruption by noise which was not present in the results reported by Lim [12].

Lim reported that a far more tonally pure and stronger signal could be realized by utilizing shorter leads made possible by the hybrid design, as opposed to the traditional implementation of using longer leads from the evaluation board with the MS3110 in the ZIF socket. This incongruence between the results of this study and those reported by Lim was the impetus for the next phase of this study.

B. LEAD LENGTH AND EVALUATION BOARD INTEGRATION

Lim previously reported a 4-fold increase in the performance of the MS3110 after reducing the lead length [12]. This portion of the study sought to validate these results. In this phase of the study, the hybrid design was not used. Instead, the MS3110 pre-packaged 16-pin SOIC was inserted directly into the commercially supplied evaluation board. The MS3110 and evaluation board was connected to the MEMS directional microphone via two sets of leads. One set of leads was relatively long (37 cm) and other relatively short (7 cm) as depicted in Figure 30. By interchanging the lead length and leaving the other experimental parameters constant, this phase of the study sought to investigate the effects of parasitic capacitance as a function of lead length. The MEMS directional microphone was connected via either the long or short leads to J3 (see Figure 31).

No external components were used in this phase of the study since they reside on the evaluation board (see Figure 31). The remainder of the experimental setup was the same as in the previous section.

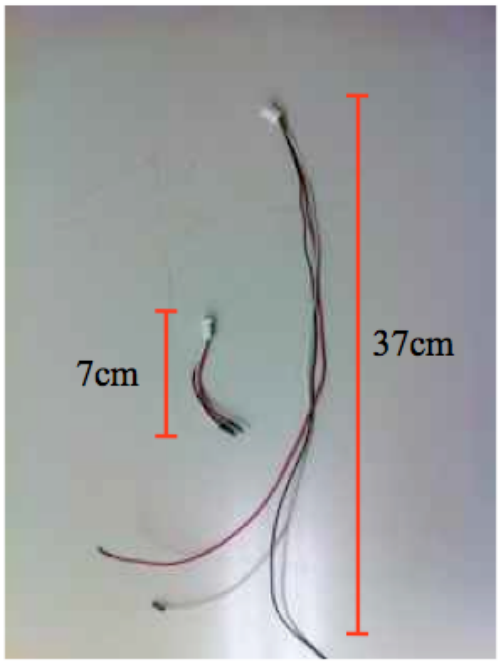

Figure 30. Both the 7cm (short) and the 37cm leads (long) are shown here.

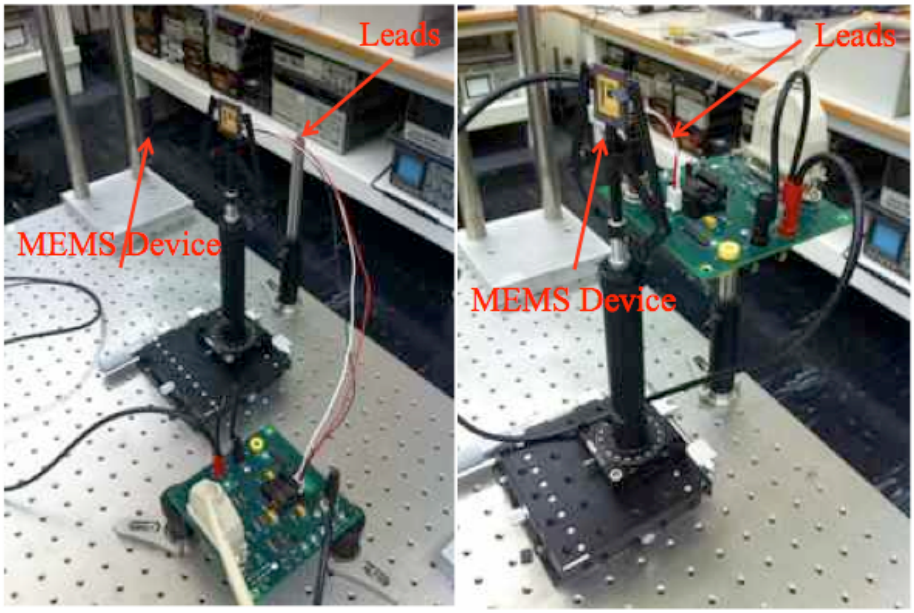

Figure 31. Both setups with the long and short leads are shown here.

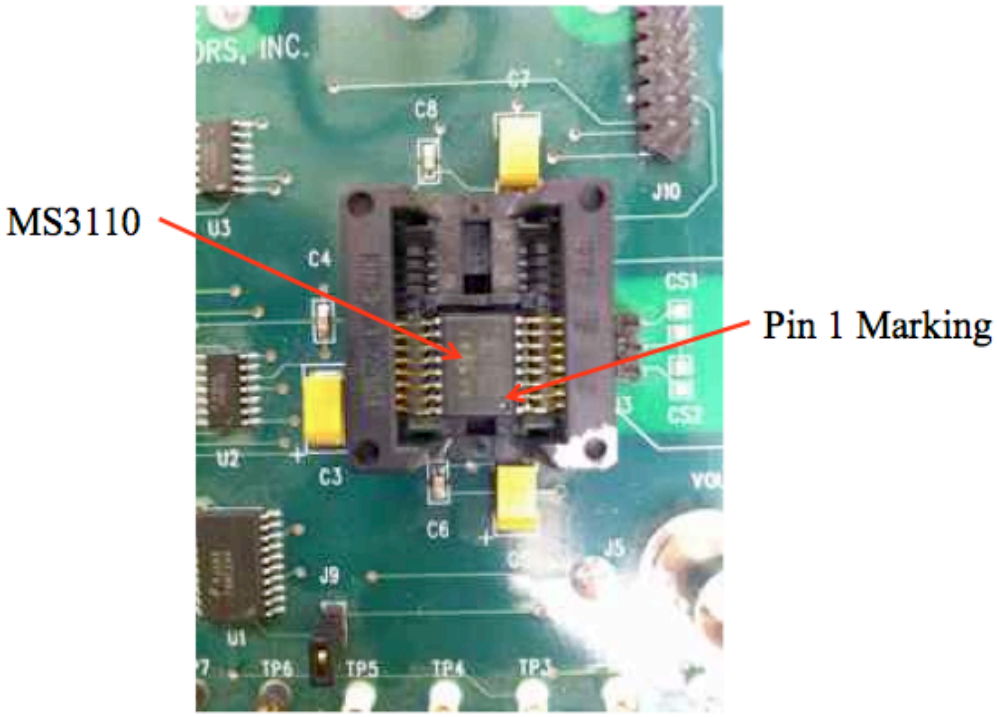

Figure 32. Here a close up of the ZIF socket is shown with the pin 1 marking in the correct place verifying the MS3110 was properly inserted.

The speaker was offset 20° from normal and the MEMS device was excited with monochromatic sound at its resonant frequency. The output was recorded both with the short and long-lead setups. The output waveform was 65 mV_{pp} with long leads (Figure 33) and 56 mV_{pp} with short leads (Figure 34). There was no noticeable improvement in waveform tonal purity moving from long leads to short leads. Overall, the results reported by Lim [12] could not be duplicated.

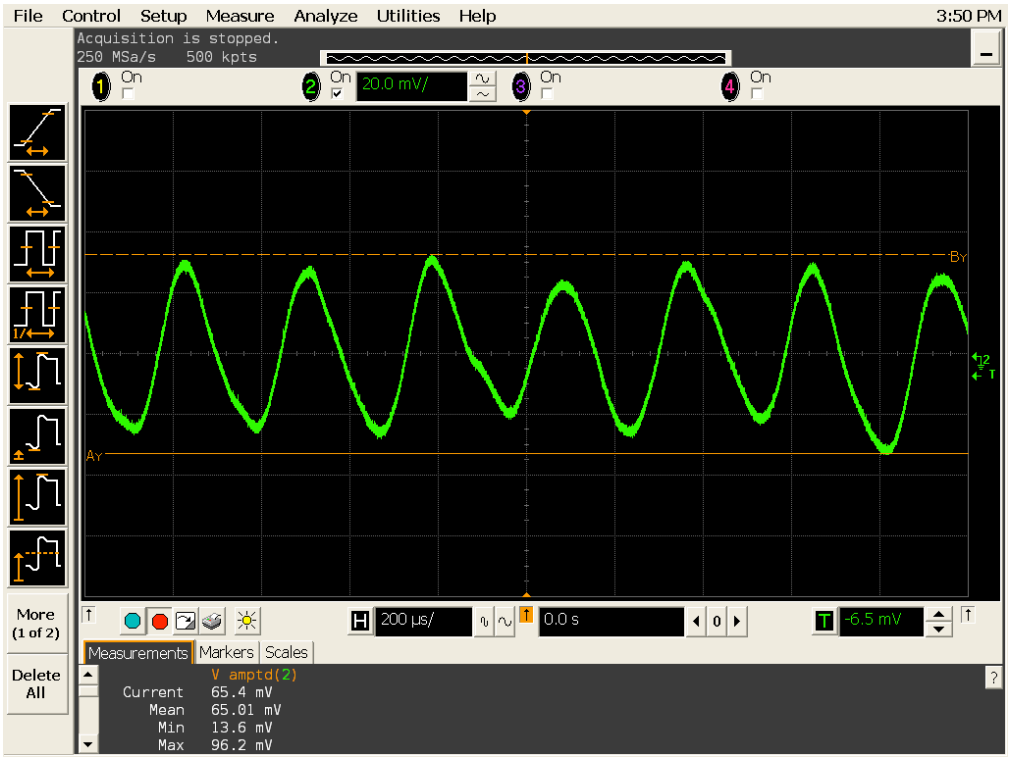

Figure 33. The observed output waveform with long leads is shown here.

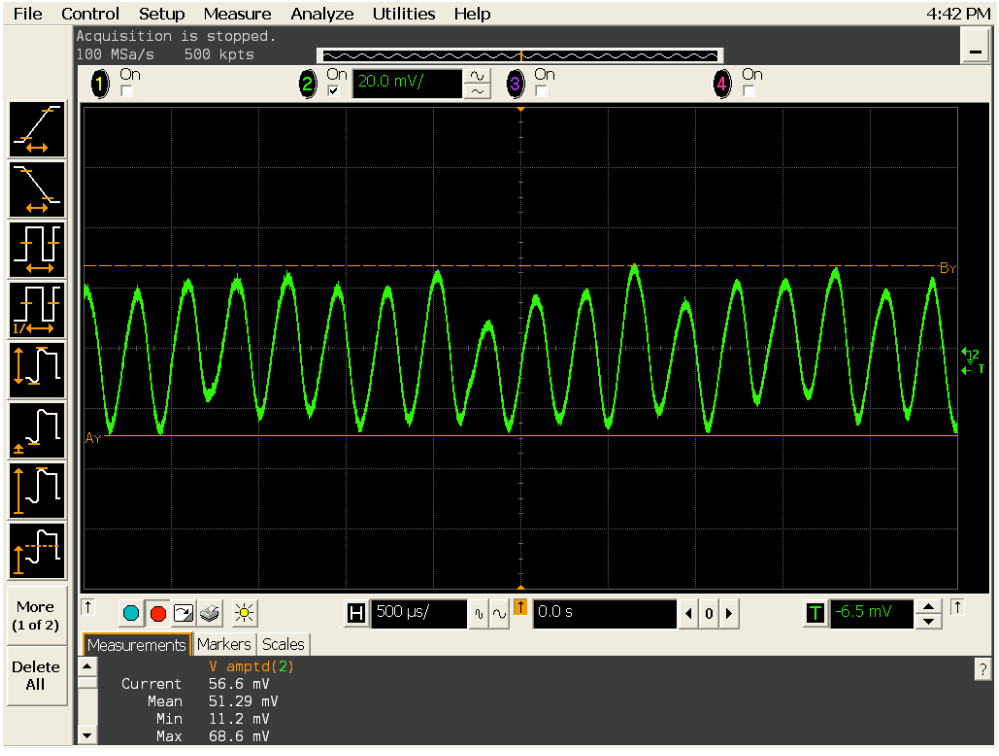

Figure 34. The observed output waveform with short leads is shown here.

C. SYSTEM NOISE

In order to better isolate the source of noise inherent in the system, the noise floor was recorded without an excitation sound signal. The mean noise floor with the long-lead setup was found to be approximately 7 mV root mean square (RMS), as shown in Figure 35. The mean noise floor with the short-lead setup was found to be approximately 3.7 mV RMS, as shown in Figure 36. The levels noted suggest that the noise can be reduced by approximately 3 dB by reducing lead length.

Next, the noise floor of the sensor was evaluated using a shielded lead roughly the same length as the long leads. Readings were taken both with the sensor connected and with two 8 pF dummy capacitors connected in place of the sensor. A RMS voltage of 1.3mV was noted with the sensor connected and a RMS voltage of approximately the same value was noted when the sensor was replaced with the dummy capacitors, as shown in Figure 37. These results suggest that unshielded leads contribute a significant amount of system noise. Further, the readings with dummy capacitors in place suggest that the sensor has minimal impact on system noise.

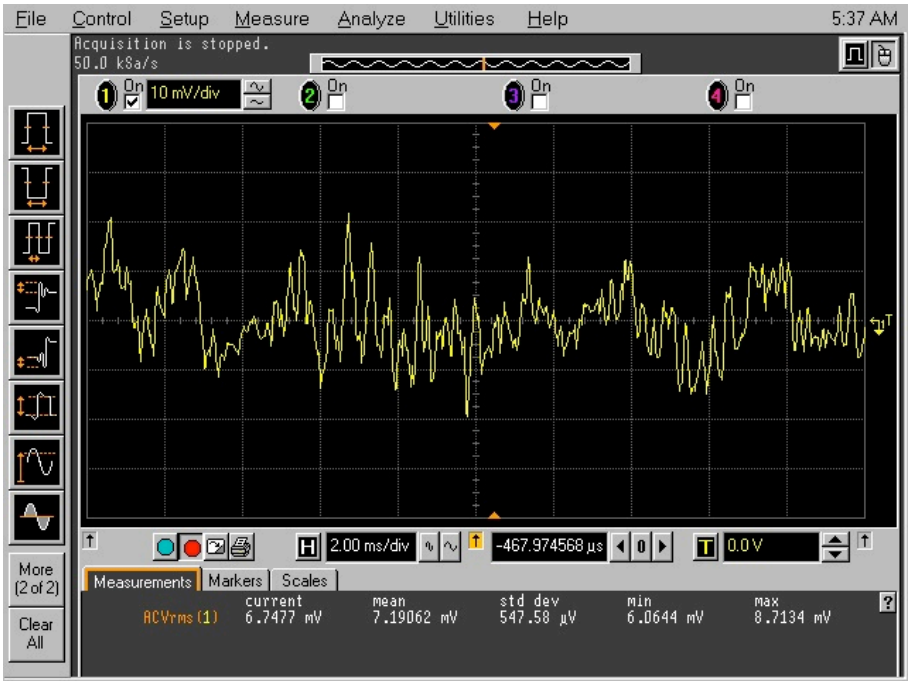

Figure 35. The noise floor with long leads exhibited the largest variance.

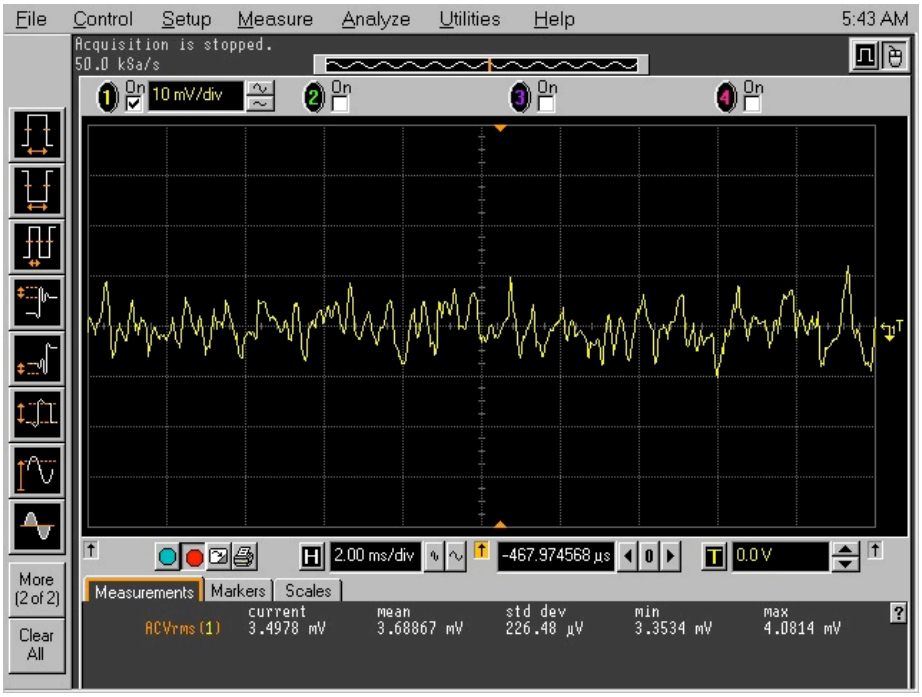

Figure 36. The noise floor with short leads showed a variance lower than the noise floor with long leads.

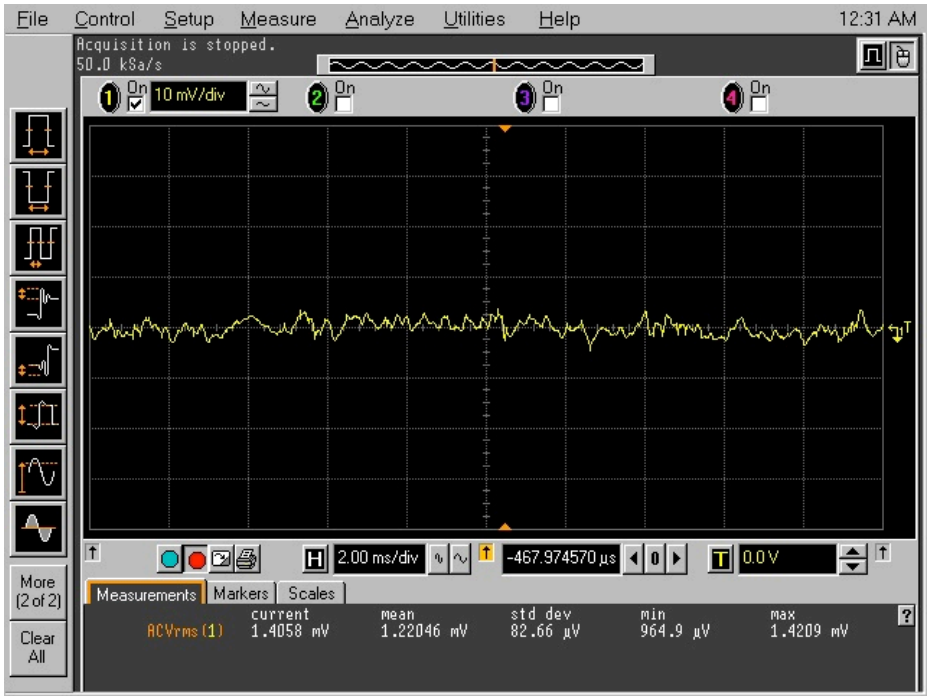

Figure 37. The noise floor with shielded leads showed a lower variance than the noise floor with unshielded leads.

D. FULL INTEGRATION

Full integration was defined by this study as mounting the readout electronic die in the same miniaturized packaging as the MEMS sensor. This study accomplished this through use of the bare-die form of the MS3110 in two phases. In the first phase, the bare die was mounted in a generic package and implemented as the prepackaged MS3110 in the hybrid setup. In the second phase, the bare die was mounted to the same generic package as the MEMS sensor and directly bonded to the sensor.

1. Bare-Die Hybrid Implementation

The die was first attached to the generic package using silver epoxy and then the die was wire bonded as described previously. Full functionality of the die was achieved and a significant output signal was realized as shown in Figure 38. Specifically, the 100 kHz square wave was observable (see Figure 39) and adjustable. The DC output voltage could be adjusted through its full range from 0V to 5V via the internal balancing capacitors, and the V2P25 reference voltage was observed within the required tolerances.

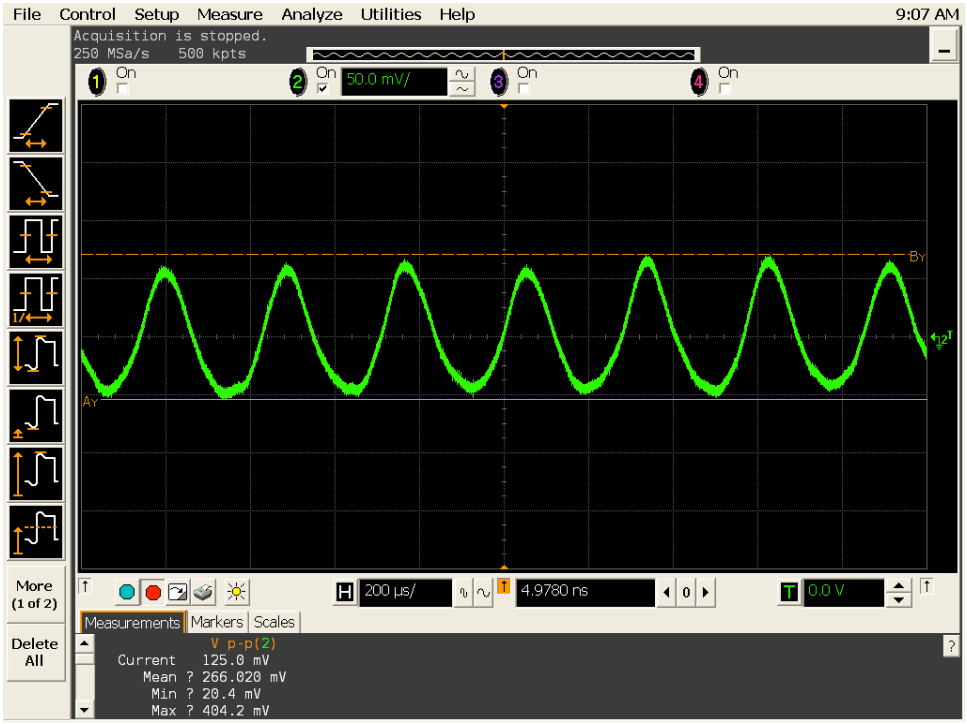

Figure 38. The observed output voltage with the MS3110 bare-die hybrid setup verified proper operation.

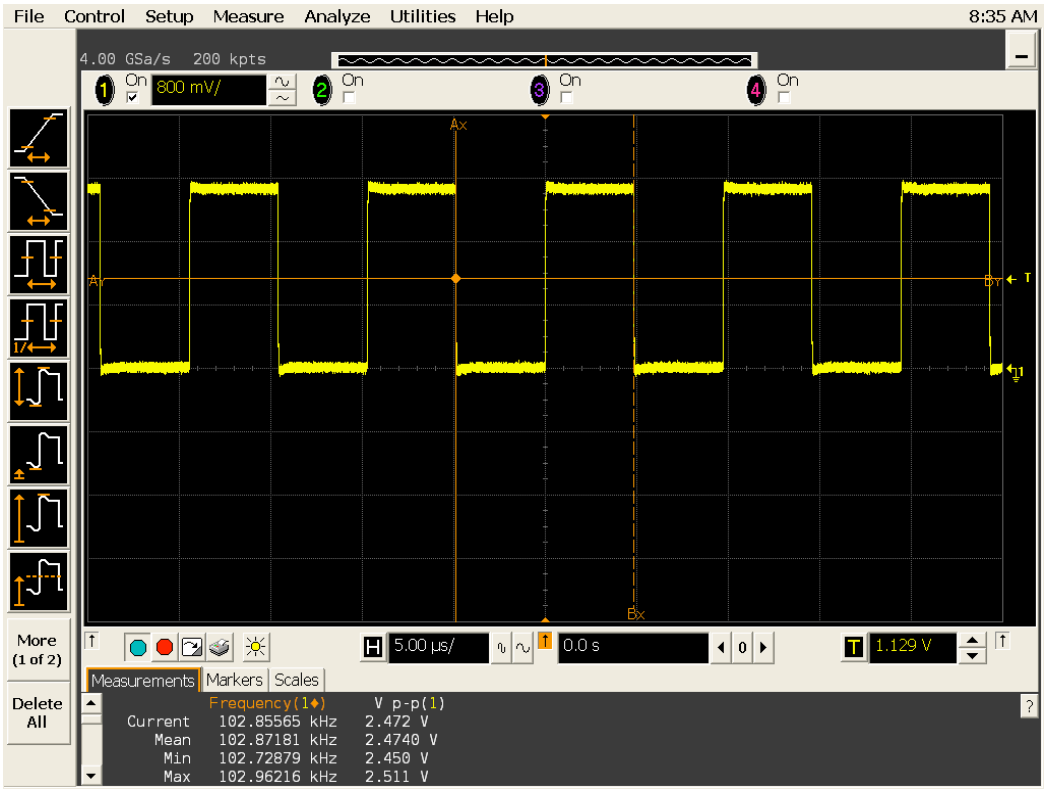

Figure 39. It was possible to observe the oscillator signal with the MS3110 bare-die hybrid setup.

2. Bare Die Full Integration

In phase two of this portion of the study, the MS3110 and the sensor were mounted together on the same carrier as shown in Figure 40. A different device (generation 6 #1) was used with a resonant frequency at approximately 5.96 kHz. In this setup, the leads from the board were all attached to the single chip carrier. The LPF was set to 5.8 kHz and the gain was set to 4 V/V. A noise-free directionally dependent output voltage was realized with no significant evidence of harmonics, as illustrated in Figure 41.

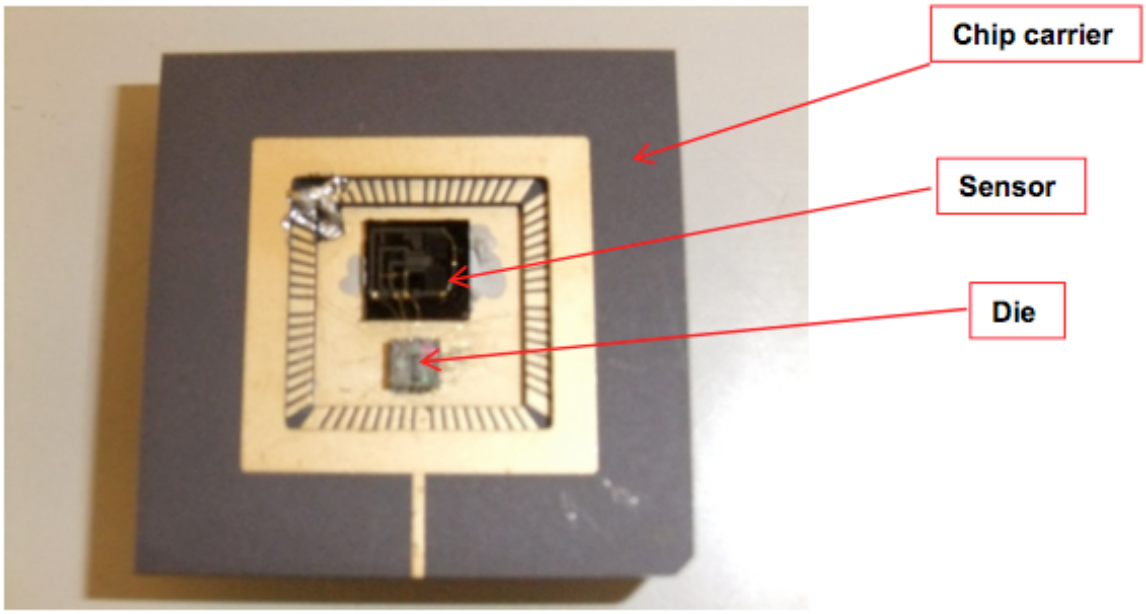

Figure 40. Here the fully integrated sensor and readout die are presented on the same package with major components annotated.

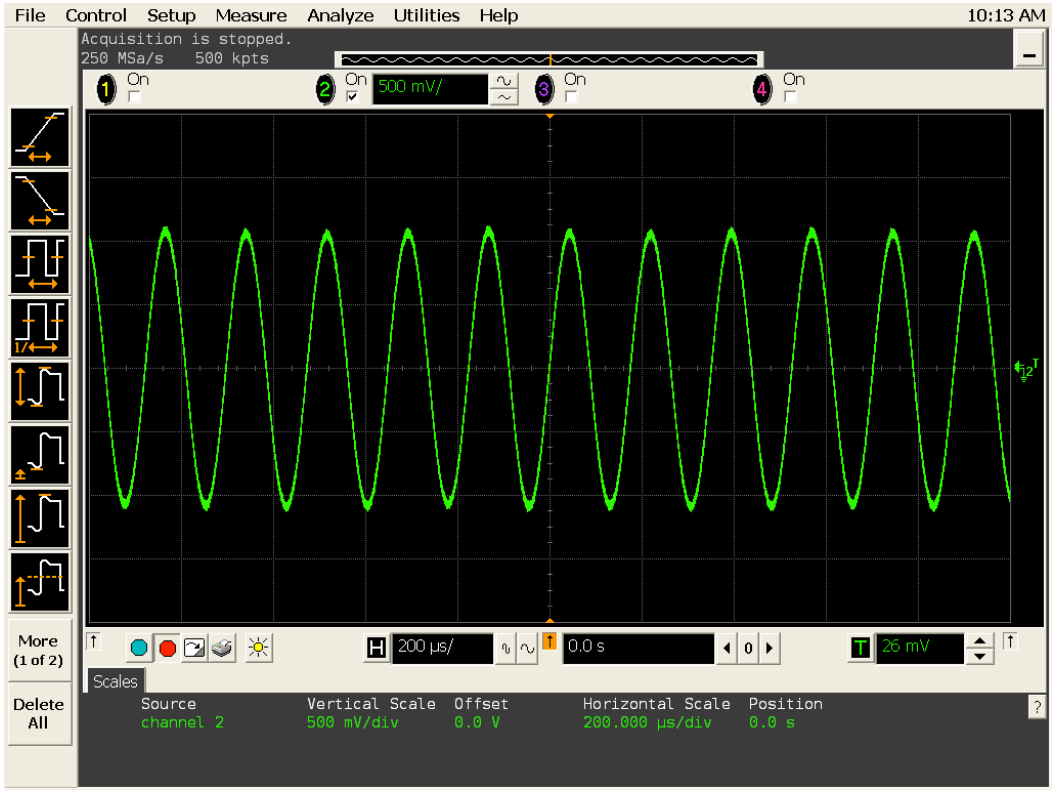

Figure 41. The response from the fully integrated sensor was notably lacking of harmonic distortion.

E. WRITING TO THE EEPROM

In the fully integrated packaging the leads connecting the MS3110 to the MEMS sensor were fixed wire bonds which gave static parasitic capacitances. Once suitable internal balancing capacitor values for the setup were identified they were solidified by writing to the MS3110 onboard EEPROM. In this manner, the device did not need to be reconfigured every time it was used.

To do this, a separate 16 V power supply was needed and was connected to the J7 banana jack of the evaluation board. It was also essential for the HV16 and WRT connections to be attached to the MS3110 from the evaluation board. After the 16 V power supply was connected, the individual settings specified by the user were loaded to the MS3110 EEPROM using the "Write EEPROM" button. When writing to the EEPROM there was not an output waveform 'jump' as there is when writing to the volatile registers. After the EEPROM write was completed the 16 V power supply was disconnected [16].

To confirm successful writing to the EEPROM, a chip reset was first issued. The chip reset caused the MS3110 to load the EEPROM contents into the control (volatile) register. Next, some of the values on the software control panel were adjusted so that they read something that should not be in the EEPROM. Finally, by clicking "Read Control Register" the software loaded the settings currently in the control register onto the control panel [16]. If the values changed to reflect what was previously written to the control register, then verification of the EEPROM control register was complete.

Once settings were written to the MS3110, several connections were not needed for operation including: SCLK, SDATA, TESTSEL, CHPRST, WRT, and HV16. Vo, V+, and V- were always necessary for proper operation. V2P25 was necessary only if there were no onboard external capacitors attached to the package. The MS3110 could now be disconnected and completely powered down. When it was reconnected and powered on, the EEPROM retained the settings last stored. Using the fully integrated design the settings in Table 2 were verified as successfully written to the EEPROM.

Table 2. The EEPROM content that was successfully written.

CF	0.513pF
CS1	2.014pF
CS2	1.083pF
Gain	4
LPF 3dB Frequency	5.8kHz

F. FULLY INTEGRATED DESIGN TEST SETUP AND RESULTS

1. Testing Setup

The performance of the fully integrated device with readout electronics was validated in an anechoic chamber. The device and a 5 V battery pack power supply was mounted to a turntable and a speaker was placed approximately two meters from the device as depicted in Figure 42. The device signal was taken through a coaxial-cable lead to ensure the purity of the output signal.

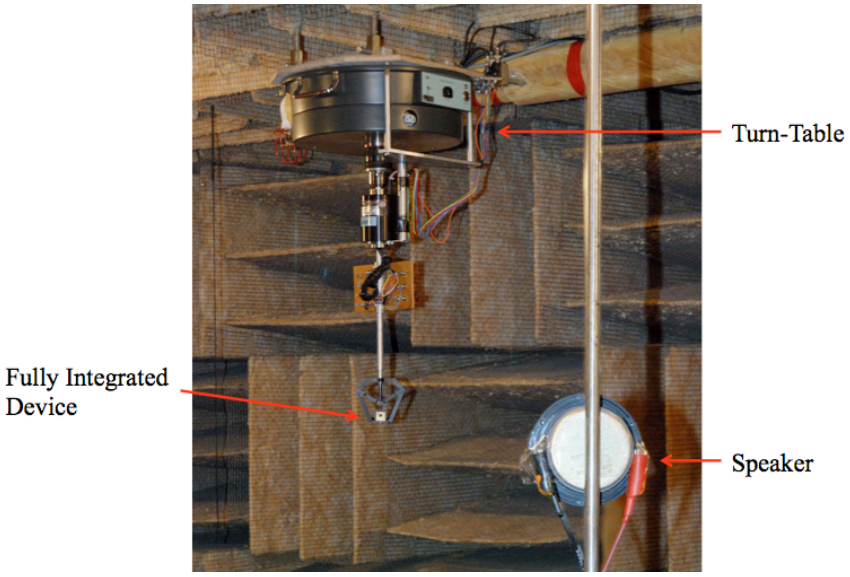

Figure 42. The experimental test setup in an anechoic chamber.

The readout was performed by taking the output waveform of the MS3110 through a pre-amplifier with unity gain and a pass band of 1 kHz to 10 kHz. The RMS value of the waveform was then tracked over time as the turntable rotated the device 360 degrees. In each case, the testing was performed while rotating the device in a single direction in order to ensure consistent results.

The bending-mode resonant frequency in the anechoic chamber was found to be very near 5.96 kHz. Tests were performed at this frequency and at 5.7 kHz. A range of sound-pressure levels were used between 45.8 dB and 80.6 dB. The upper limit on the sound-pressure level was set by the dynamic range of the speaker while the lower limit was set by the sensitivity of the device. The calculation of sound level in decibels was performed using

$$20\log\left(\frac{x\ \text{Pa}}{20\ \mu\text{Pa}}\right). \tag{III.1}$$

2. Results

The measured waveform of the device in the anechoic chamber is shown in Figure 43. Consistent with previous observations was the absence of harmonic distortion. As was reported by Touse et al., [1], [4] the magnitude of the response was observed to have a cosine dependence on angle of incidence, as illustrated in Figure 44 and 48.

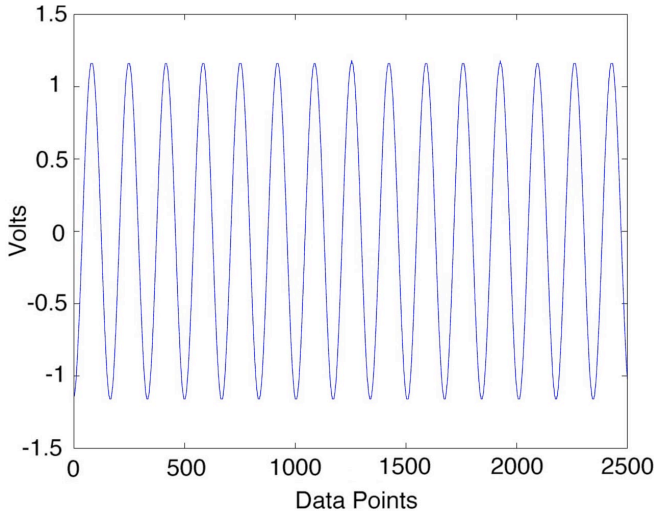

Figure 43. Measured output waveform in the anechoic chamber at 80.6 dB and 5.96kHz.

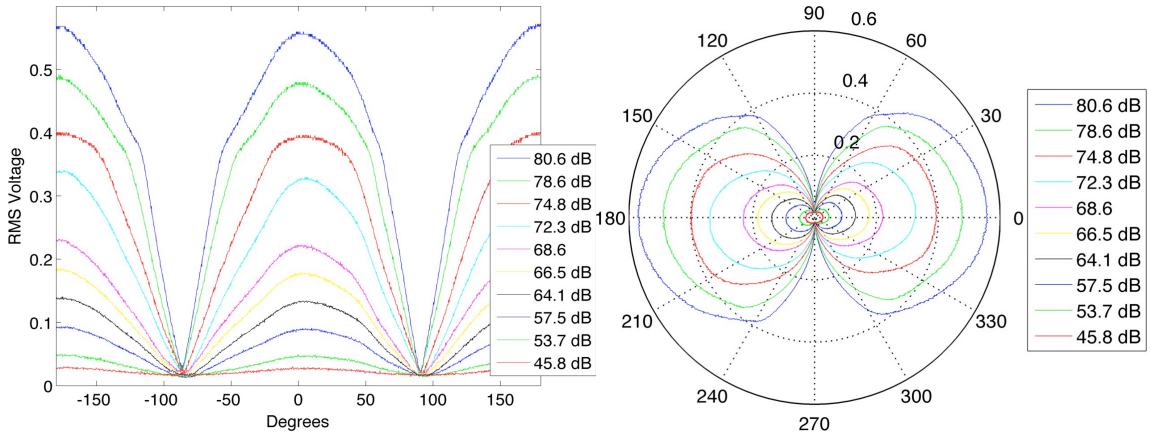

Figure 44. The measured directional response and beam pattern at 5.96 kHz and various sound-intensity levels.

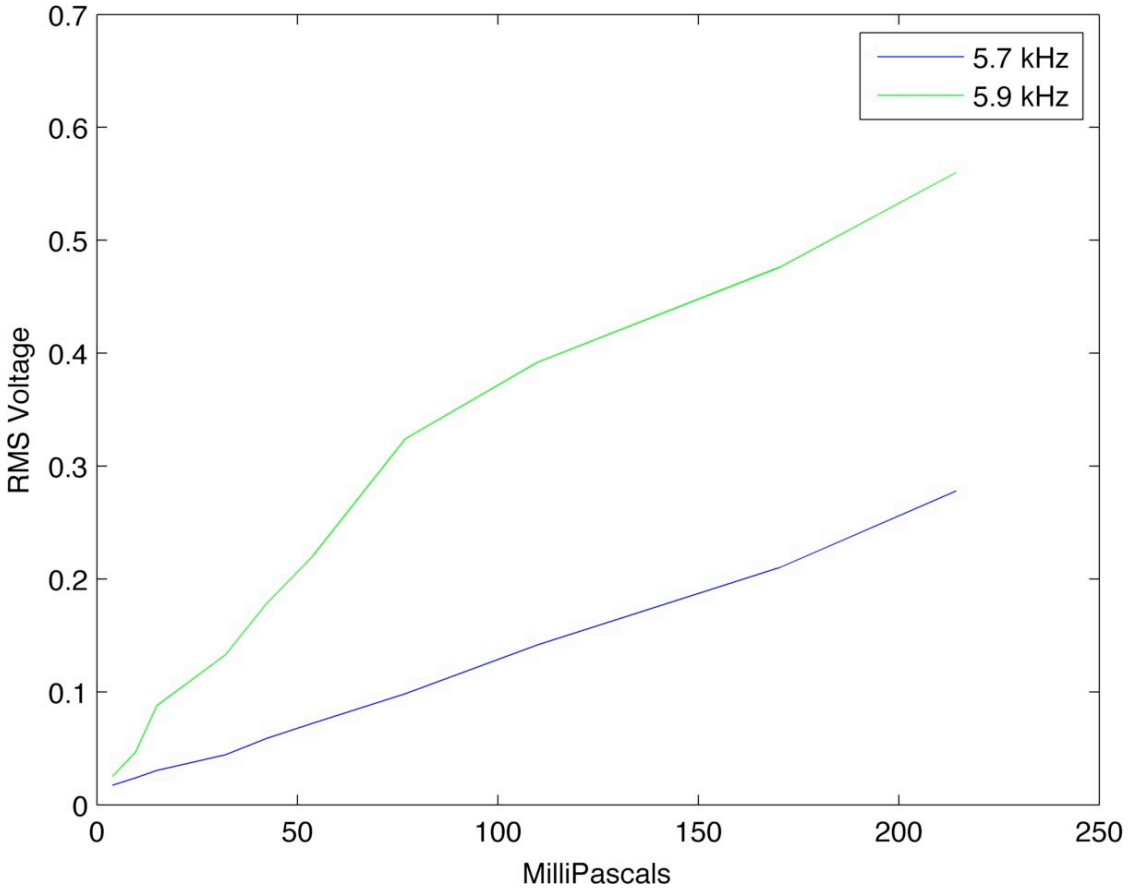

Figure 45. The sound pressure versus magnitude of the response at 5.7 and 5.96 kHz.

The magnitude of the response was approximately 3 dB lower at 5.7 kHz than it was at 5.96 kHz. A smaller response is expected since the device is excited off resonance. However, of interest was that when excited at 5.96 kHz, the magnitude of the response did not demonstrate an exact cosine dependence on angle of incidence. A distinct disturbance, shown in Figure 44, was noted at approximately -45 degrees. This disturbance was not noted at 5.7 kHz (see Figure 48). This unexpected behavior was attributed to overtaxing the amplifier in the MS3110. As the amplitude of the oscillations increased and the RMS value of the output followed, the amplifier approached its limits. This was verified by exciting the device with a directional speaker thus increasing sound intensity. The results of this trial are shown in Figure 46. The higher sound level showed very abnormal behavior at both test frequencies. When the sound level was reduced normal behavior was recovered as shown in Figure 47.

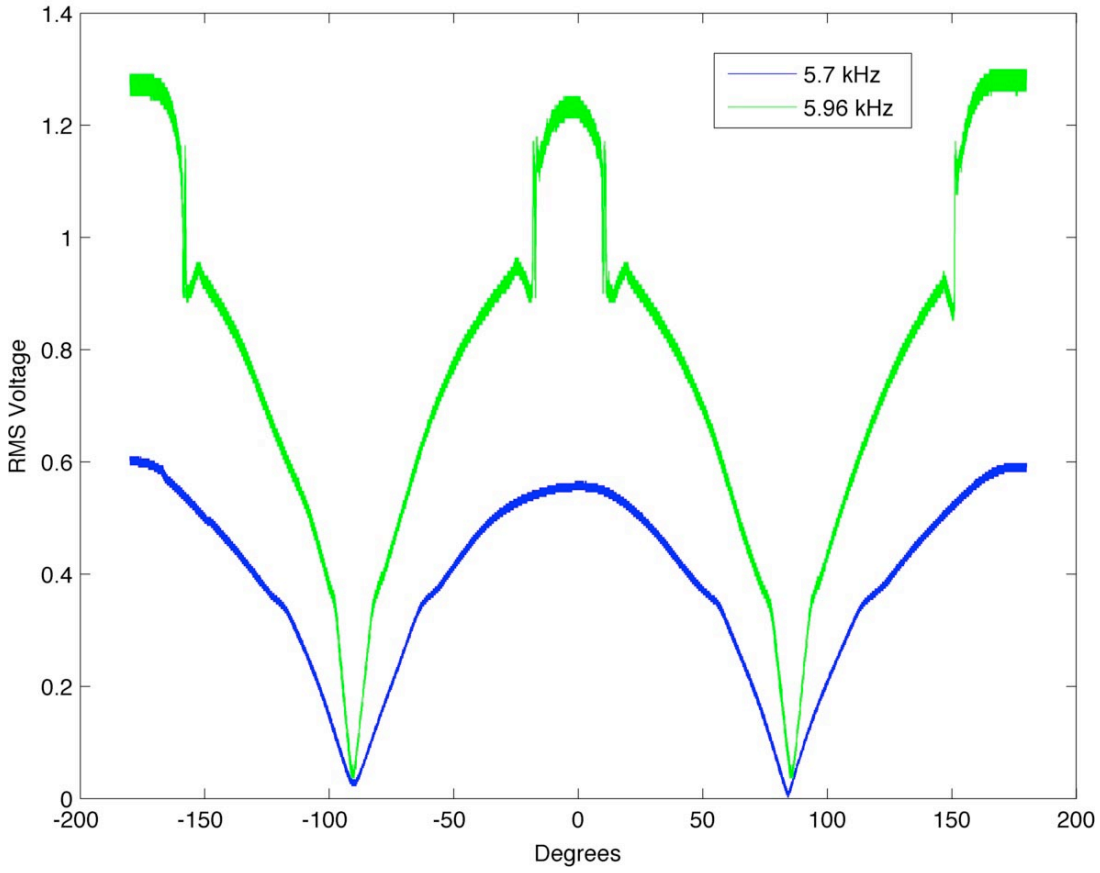

Figure 46. The device performance at high drive levels excited at both 5.7 and 5.96 kHz.

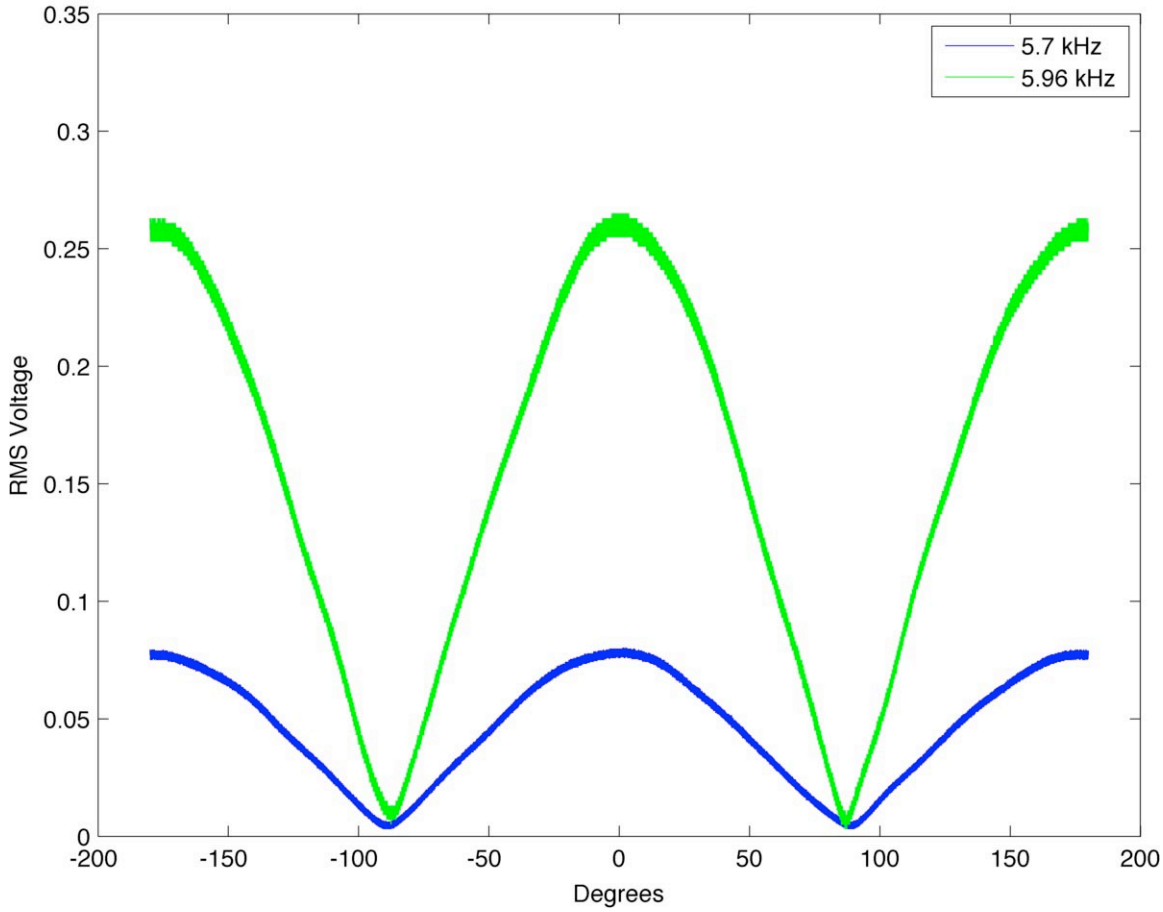

Figure 47. The device performance at low drive levels excited at both 5.7 and 5.96 kHz.

Further, the magnitude of the response, measured at its largest magnitude, was found to have a linear dependence on sound-pressure level through the range of sound pressures. As illustrated in Figure 45, the response was very linear when the device was excited by a 5.7 kHz sine wave, while some non-linearity was noticed when excited at 5.96 kHz. This abnormal behavior at 5.96 kHz, noted also in the directional response, was again attributed to an overtaxing of the MS3110 amplifier.

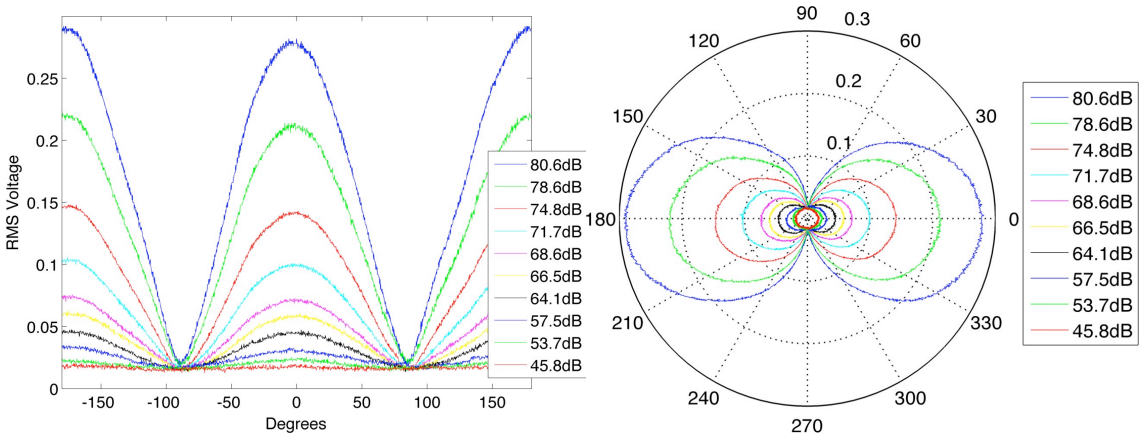

Figure 48. The measured directional response and beam pattern at 5.7 kHz and various sound-intensity levels.

In order to determine directional sensitivity, a range of ten degrees (-70 to -60 degrees) within the linear region of the directional response was chosen. This region was chosen as it provided the greatest resolution. The span of the output value corresponding to this region was used to find the device sensitivity in mV per degree. Since the recorded value was influenced by the noise floor, this final variable was used to find the resolution. With no incident sound, the noise floor was noted to have an approximate RMS voltage of 3 mV. Thus, it was assumed that ambient noise could influence the output voltage by either plus or minus 3mV resulting in 6mV of ambiguity. Device resolution followed from this ambiguity combined with the previously obtained sensitivity. This resulted in resolution as high as half a degree at a sound level of 80.6 dB and breaking down to much less accurate resolution at 53.7 dB.

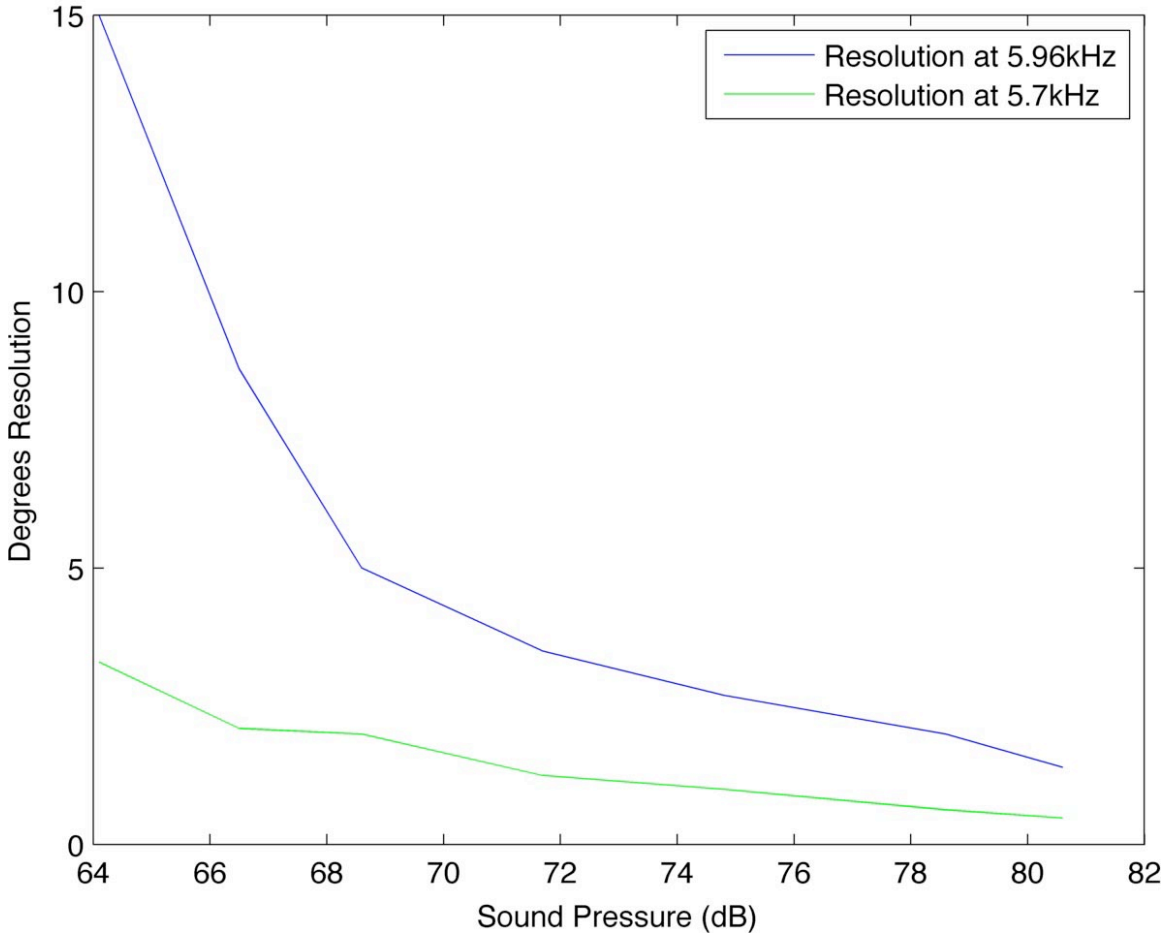

Figure 49. The recorded resolution as a function of sound pressure is shown here.

The resonant rocking-mode frequency was predicted by finite-element analysis to be at approximately 3600 Hz. The highest sound-pressure levels (80.6 dB) were used to investigate the response at this mode. After experimentation, the rocking mode proved to be too faint to observe in this experimental setup. It is, however, conceivable that a transducer designed specifically for use at the rocking mode could be used for future rocking mode analysis studies.

IV. CONCLUSION

A. SUMMARY

This study presented the detail of integrating the MS3110 Universal Capacitive Readout IC and a MEMS directional sensor. Integration methods and successful operation at various levels were discussed.

First, Lim's hybrid design was validated. The 16-pin SOIC MS3110 is capable of operating outside of the evaluation board. Lim previously reported that significantly shortening the lead length could realize a four-fold increase in the output signal due to reduced parasitic capacitances [12]. By using the exact same setup and only changing the lead length, this study could not reproduce his results.

Next, proper wiring and programming of the MS3110 bare die was demonstrated. Proper operation of the bare die MS3110 was demonstrated both in a hybrid-like design similar to the setup used by Lim and in a fully integrated single package.

Finally, proper operation of the fully integrated device was demonstrated. Two immediately obvious benefits of a fully integrated design was the ability to program settings to the EEPROM and a dramatic reduction in parasitic capacitive effects. Testing in an anechoic chamber showed very high resolution at reasonable sound levels. Finally, the design demonstrated linear performance throughout the dynamic range of the experiment when excited at 5.7 kHz.

This study took a significant step forward in preparing the sensor for production and fielding. A miniaturized sensor in acoustic detection will provide the warfighter unencumbered maneuverability and critical information necessary on today's battlefield.

B. RECOMMENDATIONS AND FUTURE WORK

Several significant steps still need to be taken in order to completely integrate the sensor into a self-sufficient package. First, in order to resolve a direction the device needs an omnidirectional microphone with which to compare its response. This level of integration has not yet been accomplished.

Currently, the sensor only has two-dimensional direction-finding capabilities. It cannot provide elevation information with only a single sensor. Further, within the two-dimensional directional resolution of the device there is still ambiguity in determining how to measure the angle of the incident sound. A multiple-device setup should be investigated to resolve these ambiguities.

Electronics to translate the output waveforms to a user-friendly interface is necessary. Since a simple output waveform is of little use to someone on the battlefield this information would ideally terminate at a simple and intuitive graphical user interface (GUI) that has yet to be investigated.

Eventually, the sensor must be a stand-alone device. In order for this to be a reality, an integrated and miniaturized power source must be developed for the sensor. The sensor must also be packaged in such a way to withstand the realities of a battlefield environment. A robust environmentally protective package must also be pursued.

A final note is that the MS3110 IAMP uses a single ended sensing design in the amplifier. This contributes common-mode noise effects to the amplifier. A differential-sensor circuit could dramatically reduce noise.

LIST OF REFERENCES

[1] M. Touse, "Design, fabrication, and characterization of a microelectromechanical directional microphone [electronic Resource]," Ph.D. dissertation, Dept. Physics, Naval Postgraduate School, Monterey, CA, 2011.

[2] Jpaur. "A gravid female Ormia ochracea resting on a fingernail" [Online]. Available: http://commons.wikimedia.org/wiki/File:Ormia_ochracea_ (gravid_female).jpg. (2010).

[3] R. N. Miles, D. Robert, and R. R. Hoy, "Mechanically coupled ears for directional hearing in the parasitoid fly ormia ochracea," *Journal of the Acoustical Society of America*, vol. 98, no. 6, p. 3059, 1995.

[4] M. Touse, J. Sinibaldi, K. Simsek, J. Catterlin, S. Harrison, and G. Karunasiri, "Fabrication of a microelectromechanical directional sound sensor with electronic readout using comb fingers," *Applied Physics Letters*, vol. 96, no. 17, 2010.

[5] A. Kinsler, G. Harnes, D. Monk, S. Wilcenski, and B. Hardy, "SOIMUMPS design handbook v.7.0," Technical report, MEMSCAP Inc., 2011.

[6] "BBN timeline" [Online]. Available: http://www.bbn.com/timeline/. [Accessed: 23 Feb. 2012].

[7] "Boomerang Warrior-X" [Online]. Available:http://www.bbn.com/ products_and_services/boomerang/boomerang_warrior_x. [Accessed: 23 Feb. 2012].

[8] S. P. Chang and M. G. Allen, "Demonstration for integrating capacitive pressure sensors with read-out circuitry on stainless steel substrate," *Sensors and Actuators, A: Physical*, vol. 116, no. 2, pp. 195–204, 2004.

[9] M. A. ERİŞMİŞ, "MEMS accelerometers and gyroscopes for inertial measurement units," M.S. thesis, Middle East Technical University, Cankaya, Ankara, Turkey, 2004.

[10] Microsensors Incorporated, "MS3110 universal capacitive readout ic pin description 16-soic and die," Costa Mesa, CA, Mar. 2006.

[11] Irvine Sensors, *MS3110 Universal Capacitive Readout IC*, Costa Mesa, CA, May 2004.

[12] C. W. Lim, "Designing an electronic readout for a directional micro electro-mechanical (mems) sound sensor," M.S. Thesis, Naval Postgraduate School, 2011.

[13] "Switched Capacitor." [Online]. In *Wikipedia*. Available: http://en.wikipedia.org/wiki/Switched_capacitor. [Accessed: 26 Nov. 2012].

[14] D. Davis, private communication, Dec. 2011.

[15] Kulicke & Soffa Industries Inc., *4500 Digital Series Manual Wire Bonders Operation and Maintenance Manual*, Singapore, Jan. 1998.

[16] Irvine Sensors, *Quick-Start Guide for the MS3110BDPC*, Costa Mesa, CA, Apr. 2004.

INITIAL DISTRIBUTION LIST

1. Defense Technical Information Center
   Ft. Belvoir, Virginia

2. Dudley Knox Library
   Naval Postgraduate School
   Monterey, California

3. Marine Corps Representative
   Naval Postgraduate School
   Monterey, California

4. Professor Clark Robertson
   Chair, Department of Electrical and Computer Engineering
   Naval Postgraduate School
   Monterey, California

5. Professor Gamani Karunasiri
   Department of Physics
   Naval Postgraduate School
   Monterey, California

6. Professor Douglas J. Fouts
   Department of Electrical and Computer Engineering
   Naval Postgraduate School
   Monterey, California

7. Professor Murali Tummala
   Department of Electrical and Computer Engineering
   Naval Postgraduate School
   Monterey, California

8. Professor Robert W. Ives
   Department of Electrical and Computer Engineering
   United States Naval Academy
   Annapolis, Maryland

9. Colonel Paul D. Montanus
   Division of Humanities and Social Sciences
   United States Naval Academy
   Annapolis, Maryland

10. Sam Barone
Department of Physics
Naval Postgraduate School
Monterey, California

11. Jay Adeff
Department of Physics
Naval Postgraduate School
Monterey, California

12. Director, Training and Education, MCCDC, Code C46
Quantico, Virginia

13. Director, Marine Corps Research Center, MCCDC, Code C40RC
Quantico, Virginia

14. Marine Corps Tactical Systems Support Activity (Attn: Operations Officer)
Camp Pendleton, California

15. Captain John D. Roth
Townsend, Tennessee